



The ^{226}Ra -Ba relationship in the North Atlantic during GEOTRACES-GA01

Emilie Le Roy¹, Virginie Sanial^{1,2,3}, Matthew A. Charette², Pieter van Beek¹, François Lacan¹,
Stéphanie H.M. Jacquet⁴, Paul B. Henderson², Marc Souhaut¹, Maribel I. García-Ibáñez⁵,
5 Catherine Jeandel¹, Fiz F. Pérez⁵, Géraldine Sarthou⁶

¹LEGOS, Laboratoire d'Études en Géophysique et Océanographie Spatiales (Université de Toulouse, CNRS/CNES/IRD/UPS), Observatoire Midi Pyrénées, 14 Avenue Edouard Belin, 31400 Toulouse, France [emilie.le.roy@legos.obs-mip.fr]

10 ²Department of Marine Chemistry and Geochemistry, Woods Hole Oceanographic Institution, Woods Hole, MA 02543, USA

³Now at Department of Marine Science, University of Southern Mississippi, Stennis Space Center, MS 39529, USA

15 ⁴Aix Marseille Université, CNRS/INSU, Université de Toulon, IRD, Mediterranean Institute of Oceanography (MIO), UM110, 13288 Marseille, France

⁵Instituto de Investigaciones Marinas, IIM-CSIC, Vigo, E36208, Spain

⁶Laboratoire des Sciences de l'Environnement Marin (LEMAR), UMR 6539, IUEM, Technopôle Brest Iroise, 29280 Plouzané, France

Correspondance to: Emilie Le Roy (emilie.le.roy@legos.obs-mip.fr)

20 **Abstract.** We report detailed sections of radium-226 (^{226}Ra , $T_{1/2} = 1602$ y) activities and barium (Ba) concentrations determined in the North Atlantic (Portugal-Greenland-Canada) in the framework of the international GEOTRACES program (GA01 section—GEOVIDE project, May-July 2014). Dissolved ^{226}Ra and Ba are strongly correlated along the GA01 section, a pattern that reflects their similar chemical behavior. Since ^{226}Ra and Ba have been widely used as tracers of water masses and ocean
25 mixing, we investigated more thoroughly their behavior in this crucial region for thermohaline circulation taking advantage of the contrasting biogeochemical patterns existing along the GA01 section. We used an Optimum Multiparameter (OMP) analysis to distinguish the relative importance of physical transport (water mass mixing) from non-conservative processes (sedimentary, river, or hydrothermal inputs; uptake by particles, and dissolved-particulate dynamics) on the ^{226}Ra and Ba
30 distributions in the North Atlantic. Results show that 72 % of the ^{226}Ra and 68 % of the Ba can be explained by conservative mixing along the section and therefore, they can be considered as conservative tracers of water mass transport in the ocean interior. However, regions where ^{226}Ra and Ba displayed non-conservative behavior were also identified, mostly at the ocean boundaries (seafloor, continental margins, and surface waters). Elevated ^{226}Ra and Ba concentrations found in deep waters of
35 the West European Basin reflect that lower North East Atlantic Deep Water (NEADWI) accumulates excess ^{226}Ra and Ba from sediment diffusion during transport. In the upper 1500 m, deficiencies in ^{226}Ra and Ba are likely explained by their incorporation in planktonic siliceous shells, or in barite (BaSO_4) (Bishop, 1988). Finally, since Ba and ^{226}Ra display different source terms (mostly deep-sea sediments for ^{226}Ra and rivers for Ba), strong decoupling between ^{226}Ra and Ba were observed at the



land-ocean boundaries. This is especially true in the shallow stations near the coasts of Greenland and Newfoundland where high $^{226}\text{Ra}/\text{Ba}$ ratios at depth reflect the diffusion of ^{226}Ra from sediment and low $^{226}\text{Ra}/\text{Ba}$ ratios in the upper water column reflect the input of Ba associated with meteoric waters.

1. Introduction

5 The primary source of radium-226 (^{226}Ra , $T_{1/2} = 1602$ y) to the ocean was found to be the diffusion from deep-sea sediments following the decay of its parent isotope, ^{230}Th (Koczy, 1958; Kröll, 1953). This mode of introduction led Koczy to use radium data to derive vertical eddy diffusivities and velocities in the deep sea (Koczy, 1958). Since then, ^{226}Ra has been widely used to study the ocean circulation and mixing at a global scale (Chung and Craig, 1980; Ku et al., 1980). In the framework of the Geochemical
10 Ocean Sections Study (GEOSECS) program, special attention was given to ^{226}Ra as its solubility and half-life made it an ideal chronometer of the global thermohaline circulation. In particular, its 1602 y half-life is more adapted than the longer half-life of carbon-14 (^{14}C , $T_{1/2}=5730$ y) that had also been used for that purpose. Therefore, the global oceanic distribution of ^{226}Ra in seawater was extensively documented throughout the major ocean basins and a unique database was generated during the
15 GEOSECS program (Broecker et al., 1970, 1967; Chung et al., 1974; Ku et al., 1970; Ku and Lin, 1976).

Barium (Ba) is an alkaline earth element like ^{226}Ra , therefore they share a similar geochemical behavior in the ocean (Chan et al., 1976; Fanning et al., 1988; Mathieu and Wolgemuth, 1973). As such, Ba was proposed as a stable analog of ^{226}Ra in order to use the $^{226}\text{Ra}/\text{Ba}$ ratio as a clock in a similar
20 manner as the $^{14}\text{C}/^{12}\text{C}$ ratio. However, the recognition that ^{226}Ra and Ba participate in upper ocean biological cycles (Ku and Luo, 1994) introduced additional complications for the use of the $^{226}\text{Ra}/\text{Ba}$ ratio as a time tracer for deep water ventilation. Both ^{226}Ra and Ba indeed increase with increasing depth, thus reflecting uptake due to biological processes in surface waters, particle scavenging and subsequent release at depth through the dissolution of the settling particles (Broecker et al., 1967; Ku et
25 al., 1970; Ku and Luo, 1994). ^{226}Ra and Ba are thus not only controlled by physical processes, but appear to be incorporated in settling particles such as calcareous and siliceous shells (Chan et al., 1976), or in barite (BaSO_4) that precipitates in the mesopelagic zone (Dehairs et al., 1980). Hence, despite different principal sources to the ocean, rivers in the case of Ba and marine sediment diffusion for ^{226}Ra , their distributions are affected by similar processes in the water column. Barium displays a linear
30 correlation with ^{226}Ra in the global ocean, resulting in a fairly constant $^{226}\text{Ra}/\text{Ba}$ ratio of 2.2 ± 0.2 dpm μmol^{-1} (dpm, disintegrations per minute)(Chan et al., 1976; Foster et al., 2004; Ku et al., 1980; Li et al., 1973; Östlund et al., 1987). Similarly, strong correlations were also found between Ba-Si (silicate) and ^{226}Ra -Si. Such relationships appeared to be more surprising because Si is not a chemical analog of Ra and Ba. It was first proposed that diatom frustules exported from the upper water column
35 could adsorb Ra and Ba, with these elements being released at depth following the dissolution of their



siliceous tests (Bishop, 1988; Chung, 1980; Dileep Kumar and Li, 1996). More recent studies showed that the similar behaviors of Ba and Si (and alkalinity) reflect similar dissolved-particulate interactions (Jeandel et al., 1996; McManus et al., 1999; Rubin et al., 2003). Indeed, Ba is not mechanistically coupled with alkalinity or silicate. Rather, the observed relationships may result from the spatial coherence of parallel carriers overprinted by hydrodynamics. The formation of biogenic silica, CaCO₃ and barite in surface water and their subsequent dissolution in the deeper water column may generate parallel oceanic distribution. While barite has been shown to be the main carrier that controls the Ba water column distribution, the relationship between Ba-Ra remains unclear.

While the global GEOSECS program provided valuable information on the coupling between biogeochemical cycles of ²²⁶Ra and Ba in the ocean, several unknowns still remain. In this work, we take advantage of a new worldwide program, known as GEOTRACES, to provide new information on the distribution of ²²⁶Ra and Ba and their relationship in the ocean. GEOTRACES program aims to characterize the distribution of trace elements and their isotopes (TEIs) (sources, sinks, internal cycling) in the ocean through a global survey consisting of ocean sections and regional process studies.

In the present study, we report dissolved ²²⁶Ra activities and dissolved Ba concentrations in the North Atlantic Ocean and Labrador Sea (GEOVIDE project, GA01 section). The North Atlantic region hosts a variety of globally significant water masses with complex circulation patterns (García-Ibáñez et al., 2015; Lherminier et al., 2010). This area is crucial for the thermohaline circulation, and thus for global climate, through its important role in the ventilation of the deep layer of the global ocean (Seager et al., 2002). As part of this process, the Meridional Overturning Circulation (MOC) includes the northward transport of warm subtropical waters. These surface waters are then cooled and transformed into subpolar waters, and may reach the Labrador and Irminger Seas where deep-water formation and deep convection take place (Bennett et al., 1985; Pickart and Spall, 2007; Yashayaev et al., 2007). We propose to study the relationship between ²²⁶Ra and Ba and to test the conservative behavior of these tracers in this specific region. We further document the Ra-Ba-Si relationship along the GA01 section, as it was done in previous sections conducted during the GEOSECS program and more recently during the GEOTRACES GA03 section.

2. Materials and Methods

2.1. Study area; the GEOVIDE project

The GEOTRACES GA01 section (GEOVIDE project; PIs : Géraldine Sarthou, LEMAR, France and Pascale Lherminier, LOPS, France) was conducted in the North Atlantic Ocean between Lisbon, Portugal, and St John's, Canada (15 May 2014-30 June 2014; Fig.1). The water samples described here were collected on board the R/V *Pourquoi Pas?*. The section crossed different topographic features and regions with contrasting biogeochemical patterns. It complemented the sections GA03 (U.S.-



GEOTRACES) and GA02 (Dutch GEOTRACES) also conducted in the Atlantic Ocean in the framework of the GEOTRACES program. Seventy-eight stations were visited during the GEOVIDE project.

2.2. Sample Collection

5 At 15 of the 78 stations completed during the GA01 cruise, up to 22 discrete 10-L seawater samples were collected through the water column from Niskin bottles. The seawater samples were passed by gravity through 10 g of acrylic fibers impregnated with MnO₂ (so called “Mn fibers”), which quantitatively adsorb radium isotopes (assumed to scavenge 100 % of Ra; (van Beek et al., 2010; Moore and Reid, 1973). High-resolution vertical profiles of ²²⁶Ra were thus built to provide a detailed ²²⁶Ra
10 section. The samples were unfiltered since particulate ²²⁶Ra activities are typically two orders of magnitude lower than the dissolved ²²⁶Ra activities (van Beek et al., 2007, 2010). From the same Niskin bottles, 15 mL was collected to determine the Ba concentration, so that Ba and ²²⁶Ra analyses were conducted from the same initial sample, which allows us to investigate the ²²⁶Ra/Ba ratio in the
15 the same seawater sample), acidified with 15 µL of HCl (10 M, Merck, Suprapur) and kept at room temperature for later analysis.

2.3. Analysis of dissolved ²²⁶Ra activities via ²²²Rn emanation

Radium-226 was determined *via* its daughter, radon-222 (²²²Rn; T_{1/2} = 3.8 days) using a radon extraction system followed by alpha scintillation counting (Key et al., 1979). The Mn Fiber samples
20 were placed into gas-tight PVC cartridges (Peterson et al., 2009) that were flushed with helium (He) for 5 min at 250 mL min⁻¹. The cartridges were sealed and held for approximately 2 weeks (minimum of 5 days) to allow for ²²²Rn ingrowth from ²²⁶Ra decay. The ²²²Rn was then flushed out from the cartridges using He and cryo-trapped in copper tubing using liquid nitrogen. The copper trap was heated to allow the ²²²Rn to be transferred to an evacuated “Lucas cells” *via* a stream of He. The “Lucas cells” are
25 tight chambers with inner walls coated with silver-activated zinc sulfide that emits photons when struck by alpha decay particles (Key et al., 1979 ; Lucas, 1957 ; Peterson et al., 2009). The cells were held 3 hours to reach the secular equilibrium of all ²²²Rn decay chain daughters. After 3 hours, the samples were counted overnight on a radon counting system (Model AC/DC-DRC-MK 10-2). The counting uncertainties (1SD, Standard Deviation) were within the range of 2–5 % for 10 L volume samples. All
30 samples were appropriately ingrowth and decay corrected. The combined Lucas cell and detector background was ~7 % of the typical total measured sample activity. The method was standardized using NIST (U.S. National Institute of Standards & Technology) ²²⁶Ra (20 dpm) sorbed onto MnO₂ fiber and analyzed in the same manner as the samples, with uncertainties (1SD) of 5 % (Charette et al., 2015; Henderson et al., 2013). Vertical profiles of ²²⁶Ra from the GEOTRACES GA01 (this study) and GA03



(Charette et al., 2015) sections that were located in close proximity off Portugal (Fig. 1) were compared, and showed a good agreement with increasing activities with increasing depth (Fig. S1).

2.4. Analysis of Dissolved Ba Concentrations

Barium concentrations were measured using an isotope dilution (ID) method (Freydier et al., 1995; Klinkhammer and Chan, 1990) by high resolution—inductively coupled plasma- mass spectrometry (HR-ICP-MS). This method was adapted to a Thermo Finnigan Element XR instrument (MIO, Marseille). The Ba measurements presented here are the sum of dissolved Ba and a very small fraction (generally <1 % of total Ba) of particulate Ba released from the samples as a result of the acidification step. Hence, while the measurements reported herein are total Ba, they are within analytical uncertainty representative of the dissolved Ba pool. The samples (0.5 mL) were spiked with 300 μL of a ^{135}Ba -enriched solution (93 % ^{135}Ba ; 95 nmol kg^{-1}) and diluted with 15 mL of acidified (2 % HNO_3 , 14 M, Optima grade) Milli-Q grade water (Millipore). The amounts of sample, spike and dilution water were assessed by weighing. The reproducibility of this method is about 1.5 % (1 RSD, Relative Standard Deviation) as tested on repeated preparations of the reference solution SLRS-5 (NRC-CNRC river water reference material for trace metals). Average Ba values obtained for SLRS-5 were $13.48 \pm 0.20 \mu\text{g L}^{-1}$ (1 σ) with RSD of 1.5 %, which is in good agreement with the certified values (SLRS-5 $13.4 \pm 0.6 \mu\text{g L}^{-1}$). The limit of detection calculated as three times the standard deviation of the procedural blank was 0.09 nmol L^{-1} .

2.5. Multiparameter Mixing Model

An Optimum MultiParameter (OMP) analysis was used to distinguish the relative importance of physical transport (i.e., water mass mixing) from non-conservative processes (input from the sediments, rivers or hydrothermal vents, dissolution of particles; uptake by particles and dissolved-particulate dynamics) on the ^{226}Ra and Ba distributions in the North Atlantic. We used the OMP analysis computed for the GA01 section by Garcia Ibanez et al., (this issue) with 12 source water types (SWTs). Based on historical data reported from the North Atlantic, we defined ^{226}Ra and Ba endmember concentrations associated with each SWT (Table S1). The characteristics of SWTs (potential temperature, salinity, and geographical location) were used to determine the SWTs endmembers for ^{226}Ra and Ba, reported by Garcia Ibanez et al., (this issue). In some cases, data from the GA01 section were used for the SWT endmember (Table S1). These ^{226}Ra and Ba SWT endmembers were then used to calculate the ^{226}Ra and Ba concentrations that strictly result from mixing of the different water masses. In this way, we estimated the conservative component of ^{226}Ra and Ba, which can in turn be compared to the *in situ* concentrations to generate the non-conservative component of ^{226}Ra and Ba along the GA01 section.

Monte Carlo perturbation experiments were conducted to evaluate the sensitivity of the results with respect to the SWT endmember variations. A total of 250 random perturbations for each SWT



endmembers were chosen in an arbitrarily range (considering perturbations up to ± 1 dpm 100 L^{-1} for ^{226}Ra and $\pm 5 \text{ nmol L}^{-1}$ for Ba). Then, for each data point of the section, the ^{226}Ra activities and Ba concentrations were calculated for each perturbation of the SWT endmembers. The resulting standard deviations on the ^{226}Ra and Ba concentrations gave information on the sensitivity of the conservative component of ^{226}Ra and Ba determined using OMP analysis. The Monte Carlo experiments allowed us to conclude that the ^{226}Ra and Ba anomalies determined from the OMP analysis can be considered as conservative within a range of ± 1 SD, which correspond to ± 0.7 dpm 100 L^{-1} for ^{226}Ra and ± 2.0 nmol L^{-1} for Ba. Outside of these ranges, ^{226}Ra and Ba were considered as non-conservative. These non-conservative values can either be positive (representative of a net addition of ^{226}Ra and Ba) or negative (representative of a net removal of ^{226}Ra and Ba).

Note that the OMP analysis was not solved where non-conservative behavior of temperature and salinity is expected: for waters above 100 m and for waters with salinities lower than 34.7. Changes in water mass properties may be due to air-sea interaction or inputs of fresh waters (i.e., near Greenland shelf; (Daniault et al., 2011)).

3. Results

3.1. Hydrodynamic context

The OMP analysis was used to identify the different water masses crossing the GA01 section. The potential temperature-salinity diagram for all the GA01 stations along with the different SWT endmembers used in the OMP analysis are represented in Fig.2. The salinity section is shown in Fig.3. The different water masses present along the GA01 section are described below.

3.1.1. Upper waters

Three main water masses were found in upper waters (<1000 m) in the investigated area (Fig.3). First, the Central Waters occupied the upper eastern part of the GA01 section from the Iberian Peninsula to the Reykjanes Ridge (stations 1 to 26). Their distribution was associated with the circulation of the North Atlantic Current (NAC). The NAC transports warm and saline waters northward, connecting the subtropical and the subpolar latitudes, and is part of the upper layer of the Atlantic Meridional Overturning Circulation (AMOC) in the North Atlantic subpolar gyre. The NAC flows eastward from the Grand Banks of Newfoundland, splitting into four branches at the Mid-Atlantic Ridge (MAR), while incorporating local water masses (Fig.1). East of the MAR, the two northern branches of the NAC flow northward into the Icelandic Basin, the Rockall Plateau and the Rockall Trough, while the two southern branches flow southward into the West European Basin. The Central Waters can be identified by the highest potential temperature of the entire GA01 section and are represented by two endmembers called



East North Atlantic Central Waters (ENACW₁₆ and ENACW₁₂). The ENACW₁₆ is warmer (16 °C) than the ENACW₁₂ that can be identified with a potential temperature of 12.3 °C (Fig.2).

Part of the Central Waters carried by the NAC recirculates toward the Iceland Basin and the Irminger Sea, leading to the formation of subpolar mode waters by mixing and cooling in the subpolar gyre (Lacan and Jeandel, 2004; McCartney, 1992). Iceland Subpolar Mode Water (IcSPMW) is formed in the Icelandic Basin and is located, along GA01, over the Reykjanes Ridges (stations 32 and 38) (Fig.3). The IcSPMW is described by two endmembers, the SPMW₇ and the SPMW₈, which are distinguished by their potential temperature of 7.0 °C and 8.0 °C, respectively (Fig.2). Once formed, the IcSPMW follows the Irminger Current.

Finally, the Irminger Subpolar Mode Water (IrSPMW) is the result of the transformation of the Central Waters and the IcSPMW, and is formed northwest of the Irminger Sea (Krauss, 1995). The IrSPMW is located near Greenland (stations 53, 57 and 60) (Fig.3)(García-Ibáñez et al., 2015; Lacan and Jeandel, 2004; Read, 2000).

3.1.2. Intermediate waters

The Subarctic Intermediate Water (SAIW) originates in the Labrador Current (Read, 2000). The SAIW is associated with the advection of waters from the Labrador Sea within the NAC; it subducts below the Central Waters at approximately 600 m. Low salinities (34.8 and 34.7) and potential temperatures of 4.5 °C and 6 °C are representative of the two SAIWs, SAIW₄ and SAIW₆, respectively (Fig.2).

Around the Rockall Plateau, the SAIW overlies the Mediterranean Water (MW). The MW enters the North Atlantic through the Gibraltar Strait and flows northward while extending westward. The MW can be identified in the West European Basin at approximately 1200 m (stations 1 and 13 in Fig.3) with a salinity of 36.5 (Fig.2)(García-Ibáñez et al., 2015).

The Labrador Sea water (LSW) is found in multiple locations and at different water depths along the GA01 section (Fig.3). The LSW is formed by progressive cooling and freshening in winter due to deep convection. The LSW can be characterized by its minimum salinity (34.87) and its minimum potential temperature (3 °C) (Fig.2). The LSW contributes to the stratification of the interior of the North Atlantic and its boundary currents and spreads at intermediate depths in three different basins intersected by the GA01 section (Fig.1). The three independent pathways are: (i) northward into the Irminger Sea (station 44), (ii) eastward across the MAR, through the Charlie-Gibbs fracture zone, then northward into the Iceland Basin (station 32) and eastward into the West European Basin (stations 21 and 26), and (iii) equatorward as a major component of the North Atlantic Deep Water in the Deep Western Boundary Current (DWBC), which constitutes the lower limb of the AMOC. Along these paths, the LSW mixes with both the overlying and underlying water masses and becomes warmer and saltier (Lazier, 1973).



The Polar Intermediate Water (PIW) is characterized by very low salinity (34.9) and potential temperature (less than 2 °C) (Fig.2) and is defined as a separate upper core on the Greenland slope. The PIW is episodically injected into the Irminger Sea and originates from either the Arctic Ocean or the Greenland shelf (Falina et al., 2012; Jenkins et al., 2015; Rudels et al., 2002).

5 3.1.3. Overflow waters and deep waters

The Iceland—Scotland Overflow Water (ISOW) originates at the Iceland-Scotland sill, and entrains the overlying warm saline Atlantic waters (SPMW and LSW). ISOW identification features are a potential temperature of 2.6 °C and a salinity of 34.98 (Fig.2(van Aken and Becker, 1996)). ISOW was found at stations located on the Eastern flank of the Reykjanes Ridge (stations 32 and 38) and near
10 Greenland (stations 60 and 64) at great depth (2000–3500 m) (Fig.3).

Overflow waters coming from the Denmark Strait mix with both the SPMW and the LSW during descent into the Irminger Sea to form the Denmark Strait Overflow Water (DSOW) (Fig.1) (Read, 2000; Yashayaev and Dickson, 2008). DSOW is located at the northern end of the Irminger Sea (station 44) and occupies the deepest part of the Greenland continental slope (stations 69 and 77)
15 (Fig.3). At bottom depth, DSOW is easily identified by a minimum potential temperature of 1.3 °C (Fig.2).

In the Southern Ocean, the Antarctic Bottom water (AABW) is formed by deep winter convection of surface waters. AABW flows to the north along the eastern side of the Atlantic and contributes to the formation of the lower North East Atlantic Deep Water (NEADW) once this water penetrates the
20 Iberian Abyssal Plain (Fig.1). The NEADW is laying at the bottom of the West European Basin (stations 1 to 26 in Fig.3) with a mean salinity of 34.895 and a potential temperature of 1.98 °C (Fig.2). Then, the NEADW recirculates into the Rockall Trough and meets ISOW in the Iceland Basin (van Aken, 2000; McCartney, 1992; Schmitz and McCartney, 1993).

3.2. Distribution of ²²⁶Ra and Ba along the GA01 section

25 The ²²⁶Ra distribution for the GA01 section is presented in Fig.4 with Ba concentrations overlain. The ²²⁶Ra activities and Ba concentrations in the water column range from 7 to 25 dpm 100 L⁻¹ and from 33.6 to 81.5 nmol L⁻¹, respectively. These data are in good agreement with Atlantic data from the GEOSECS program, which range from 6.8 to 23.4 dpm 100 L⁻¹ for ²²⁶Ra and from 35 to 105 nmol L⁻¹ for Ba (Broecker et al., 1976).

30 For both ²²⁶Ra and Ba, the vertical gradient is stronger in the eastern part of the section (West European Basin) than on the western part of the section (from Reykjanes Ridge to Newfoundland). Both are particularly high near the seafloor in the West European Basin (²²⁶Ra: 14 - 25 dpm 100 L⁻¹; Ba: 63 - 82 nmol L⁻¹) and are in agreement with data previously reported for this region (Broecker et al., 1976; Charette et al., 2015). At intermediate depths, Ba concentrations range from 40 to 50 nmol L⁻¹ in



the West European Basin (stations 1 and 21) and ^{226}Ra activities range from 9.5 to 10.9 dpm 100 L⁻¹, also in good agreement with literature data (Charette et al., 2015; Schmidt and Reyss, 1996). Low ^{226}Ra and Ba are found in upper waters of the West European Basin and the Iceland Basin (8.1 - 8.9 dpm 100 L⁻¹ and 35- 43 nmol L⁻¹, respectively). Intermediate ^{226}Ra activities and Ba concentrations (9 dpm 100 L⁻¹ and 42 nmol L⁻¹, respectively) are observed in bottom waters in Irminger and Labrador Seas. Between the Reykjanes Ridge and Newfoundland, ^{226}Ra activities range between 7–10 dpm 100 L⁻¹ in surface and intermediate waters. Similar to ^{226}Ra , Ba concentrations are relatively low in this area, ranging from 39–50 nmol L⁻¹. The distributions in ^{226}Ra and Ba are to a first order explained by the different water masses present in the region, as discussed below.

10 4. Discussion

4.1. ^{226}Ra -Ba and ^{226}Ra -Ba-Si relationships

A linear correlation between ^{226}Ra and Ba is observed for all data collected along the GA01 section (Fig.5). The slope of the ^{226}Ra -Ba linear regression obtained by this study in the North Atlantic is 2.5 ± 0.1 (2SD) dpm μmol^{-1} which agrees with the slope of the ^{226}Ra -Ba linear regression of 2.3 dpm μmol^{-1} reported during the GEOSECS program for all the oceanic basins (Chan et al., 1976). The intercept on the horizontal Ba axis is 4.4 nmol L⁻¹ for the GA01 section, which is in agreement with GEOSECS data (Chan et al., 1976; Li et al., 1973). This positive intercept may be the result a greater input of ^{226}Ra relative to Ba close to bottom sediments and a larger riverine Ba input relative to ^{226}Ra (Ku and Luo, 1994). The slope of the ^{226}Ra -Ba linear regression reported from the GEOSECS program is similar from one oceanic basin to the other. The ^{226}Ra /Ba ratio (slightly different from the slope) is also fairly constant throughout the global ocean (2.2 ± 0.2 dpm μmol^{-1} ; Östlund et al., 1987). This pattern indicates that ^{226}Ra and Ba behave similarly in the ocean. Since ^{226}Ra and Ba are incorporated in settling particles such as calcareous and siliceous shells, or barite (BaSO₄), and are then released at depth following the dissolution of these particles, the constant ^{226}Ra /Ba ratio suggests small fractionation between ^{226}Ra and Ba during these processes.

Investigations conducted during the GEOSECS program further concluded that ^{226}Ra and Ba were tightly correlated to orthosilicic acid (Si(OH)₄) (Chan et al., 1976; Chung, 1980; Ku et al., 1970; Ku and Lin, 1976) despite the fact that ^{226}Ra , Ba, and Si(OH)₄ exhibit different chemical behavior in the water column and different source terms. A Ra-Ba-Si relationship is also observed along the GA01 section (Fig.5). Si(OH)₄ concentrations generally increase with increasing depth, with a steeper gradient in the West European Basin (Introduction Paper, 2017; This issue), as it was also the case for ^{226}Ra and Ba (Fig.S1).



The link between ^{226}Ra , Ba and Si has been shown to reflect parallel dissolved-particulate interactions between barite and biogenic silica (Bishop, 1988; Chung, 1980; Jacquet et al., 2005, 2007; Jeandel et al., 1996), the main carrier of Ra in the ocean remains an open question.

In contrast to the ^{226}Ra -Ba relationship, the slope of the ^{226}Ra -Si(OH)₄ relationship during
5 GEOSECS exhibited significant spatial variability from one oceanic basin to the other (Li et al., 1973). In the case of GA01, the ^{226}Ra -Si(OH)₄ linear regression slope is 2.4 ± 0.9 (2SD) 10^3 dpm mol⁻¹. As a comparison, the ^{226}Ra -Si(OH)₄ slope reported for the GEOTRACES-GA03 section conducted south of the GA01 section in the Atlantic Ocean was $2.1 \cdot 10^3$ dpm mol⁻¹ (Charette et al., 2015). As a comparison, the slope of the ^{226}Ra -Si(OH)₄ linear regression is $34.3 \cdot 10^3$ dpm mol⁻¹ in the Pacific ocean and 14.5
10 10^3 dpm mol⁻¹ in the Antarctic Ocean. The ^{226}Ra -Si(OH)₄ relationship has an intercept with the vertical axis of 7.3 ± 0.1 dpm 100 L^{-1} , which represents the residual ^{226}Ra resulting from the total usage of Si in surface waters (Ku et al., 1970). According to (Shannon and Cherry, 1971), the removal of ^{226}Ra in the upper waters is limited by Si. For both the ^{226}Ra -Ba and ^{226}Ra -Si(OH)₄ relationships, several values are clearly outside of the linear regression trend (Fig.5), a pattern that indicates deviation from the
15 relationship usually observed between ^{226}Ra and Ba (or Si(OH)₄). Such deviations may result from non-conservative processes.

4.2. ^{226}Ra and Ba distributions and their relationship with hydrography

A striking feature of the GA01 section is that the ^{226}Ra activities and Ba concentrations are particularly high in the West European Basin below 2000 m (Fig.4), due to the presence of the
20 NEADWI, which includes waters with a southern origin (Read, 2000). South of the Antarctic Convergence, the surface waters contain high ^{226}Ra activities from the upwelling of deep waters enriched in ^{226}Ra associated with the circumpolar current (Ku and Lin, 1976). These waters then sink and circulate northward into the Atlantic Ocean. (Broecker et al., 1976) showed that the decrease in the ^{226}Ra activities from south to north is produced by the mixing of the AABW and bottom waters of
25 northern origin. Figure 6 was computed combining GEOSECS and TTO data (^{226}Ra , Si(OH)₄, salinity and temperature) gathered in the AABW that travels northward between 60°S and 40°N. The same data (^{226}Ra , Si(OH)₄, salinity and temperature) determined in the NEADWI along GA01 are also reported. Following the AABW, between 60 °S and the equator, the high ^{226}Ra activities are associated with relatively low salinity and temperature, and high Si(OH)₄ (Fig.6). Then, while crossing the Mid-Atlantic
30 Ridge at the equator and at 11 °N, the AABW goes through an important transformation: ^{226}Ra activities and Si(OH)₄ concentrations decrease while salinity and temperature tends to increase (Fig.6). The ^{226}Ra and Ba endmembers for the NEADWI were chosen at this specific location to coincide with the NEADWI endmembers used for the OMP analysis (Fig.6; Fig.S2). When reaching the latitude of ca. 40 °N, these waters are then characterized by high ^{226}Ra activities compared to the waters located in the
35 eastern part the GA01 section. This pattern can also be observed in the GA03 section conducted south



of the GA01 section (Charette et al., 2015), the two sections being separated by only ca. 500 km in that basin.

In contrast, the lowest ^{226}Ra activities and Ba concentrations reported on the GA01 section are associated with the Central Waters (upper waters of the West European Basin; Fig.4). Central Waters are derived from the NAC and mix with the SAIW and the SPMW. Along their path, Central Waters remain in the upper water column, and therefore are not affected by the deep sedimentary source of ^{226}Ra . West of the Iceland Basin between 200 and 400 m (stations 32 and 38), an increase in the ^{226}Ra activities and Ba concentrations is associated with the IcSPMW.

A slight increase in ^{226}Ra is observed between 1000–1600 m in the West European Basin (Fig.4; Stations 1 and 13) where a salinity maximum is identified. This pattern is associated with the MW. This is corroborated by the slightly higher Ba concentrations and lower $^{226}\text{Ra}/\text{Ba}$ ratios, as observed in the Western Mediterranean Sea (van Beek et al., 2009), spreading westward. At these depths, the OMP analysis confirms the presence of the MW at about 41 % - 66 % (stations 1 and 21; Garcia Ibanez et al., 2017; this issue).

Relatively uniform and low ^{226}Ra activities and Ba concentrations are found between the surface and 2500 m in the Labrador Sea, up to 2000 m in the Iceland Basin and deeper in the Irminger Basin (Fig.5). These distributions can be related to the LSW which is formed by winter convection in the Labrador Sea (Fröb et al., 2016; Pickart et al., 2003; Yashayaev and Loder, 2016). When formed, the LSW transports the low ^{226}Ra activities and Ba concentrations characteristic of surface waters to the deep ocean. The LSW then spreads into the Irminger and the Iceland Basin while conserving its low ^{226}Ra and Ba signatures. Relatively low ^{226}Ra activities and Ba concentrations are found at bottom depths in the Irminger and Labrador Seas and may be associated with DSOW, which is also a recently ventilated water mass (Lazier, 1973).

Finally, according to the OMP analysis, ISOW is present at several stations along the GA01 section (Garcia-Ibanez et al., 2017, this issue). First, on the eastern flank of the Reykjanes Ridge (station 32), 60 % of the water between 2700 and 3000 m is considered as ISOW. Then, in the Labrador Sea (stations 69 and 77), an average of 54 % of the water between 2100 and 3000 m is identified as ISOW. The slight increase in ^{226}Ra activities and Ba concentrations observed at these locations may thus be related to the ISOW.

4.3. Conservative versus non-conservative behavior of ^{226}Ra and Ba

The use of an Optimum Multiparameter (OMP) analysis allowed us to distinguish the relative importance of physical transport (i.e., mixing of water masses) from non-conservative processes on the ^{226}Ra and Ba distributions in the North Atlantic (Fig.7). The OMP analysis reveals that 72 % of ^{226}Ra can be considered as conservative (activities due to mixing and transport) along the GA01 section (72 % of the ^{226}Ra anomalies are within the [-0.7 and 0.7 dpm 100 L⁻¹] interval), whereas 68 % of the Ba can



be considered as conservative (68 % of the Ba anomalies are within the $[-2.0$ and $2.0 \text{ nmol L}^{-1}]$ interval). Thus, ^{226}Ra and Ba are predominantly conservative at intermediate depths: mostly between 500 m to 2000 m, but slightly deeper in the center of deep basins such as at stations 21, 44 and 69 (Fig.7). These locations correspond to the depths where the waters are far from the main sources and

5 sinks of ^{226}Ra and Ba. The non-conservative ^{226}Ra (28 % of the ^{226}Ra) is mostly distributed close to the interfaces such as surface/subsurface waters and bottom waters (both in the deep West European Basin and the Labrador Sea), near the main sources (seafloor or shallow sediments deposited onto the margins). The non-conservative Ba is mostly distributed in the upper 1500 m and in the deep West European Basin (Fig.7).

10 The discrepancy between the vertical profiles of ^{226}Ra and Ba determined along the GA01 section, and those derived from OMP analysis (Fig.8) clearly indicates deviations from the conservative behavior and reflects either an input of ^{226}Ra or Ba (positive anomalies highlighted in red; same color code as in Fig.7) or a removal of ^{226}Ra or Ba (negative anomalies highlighted in blue; same color code as in Fig.8). The $^{226}\text{Ra}/\text{Ba}$ ratios determined throughout the water column are also reported and can be

15 compared to the $2.2 \pm 0.2 \text{ dpm } \mu\text{mol}^{-1}$ value, which is the mean ratio determined during the GEOSECS program (Östlund et al., 1987) and is also the mean ratio determined along the GA01 section. 77 % of the $^{226}\text{Ra}/\text{Ba}$ ratios determined along the GA01 section are within the confidence interval $[2.0\text{-}2.4 \text{ dpm } \mu\text{mol}^{-1}]$, indicating little deviation from the mean ratio, a pattern that is associated with the similar chemical behavior between ^{226}Ra and Ba.

20 4.3.1. ^{226}Ra inputs and their relationship with Ba

Deep waters of the West European Basin display positive ^{226}Ra and Ba anomalies (stations 1 to 26; Fig.8). The ^{226}Ra anomalies are initiated at shallower depths (ca. 300-2000 m) than the Ba anomalies (ca. 1000-2000 m) (Fig.8). Between 11°N and the GA01 section (Fig.6), salinity, temperature, and $\text{Si}(\text{OH})_4$ concentrations display relatively constant trends indicating no major

25 modifications of the NEADWI along its northward transport. In contrast, the ^{226}Ra activities display a significant spatial variability north of 11°N , and clearly increase towards the north (Fig.6). This increase is decoupled from salinity, temperature, and $\text{Si}(\text{OH})_4$, was also shown by the positive anomalies deduced from the OMP analysis (Fig.8). The ^{226}Ra anomalies observed in the West European Basin may thus be explained by inputs of ^{226}Ra along the northward transport of these waters.

30 The positive anomalies result from the input of ^{226}Ra (and Ba) following either i) dissolution/remineralization of settling particles that incorporated ^{226}Ra and Ba in the upper water column (this includes the dissolution of barite, since the waters of Atlantic Ocean are undersaturated with respect to barite (Monnin et al., 1999) and/or ii) diffusion of ^{226}Ra and Ba from deep-sea sediments (Cochran and Krishnaswami, 1980) (see 4.4). Of special note are stations in the West European Basin,

35 which are especially deep (down to 5500 m). Deep sediments generally display elevated ^{230}Th activities



due to scavenging of ^{230}Th from the entire water column (Bacon and Anderson, 1982; Nozaki, 1984). The highest dissolved ^{230}Th activities reported along the GA01 section were thus observed in the deep waters of the West European Basin (Deng et al., 2017, this issue). Consequently, because ^{226}Ra is produced by the decay of ^{230}Th in the sediment, the ^{226}Ra diffusive flux in this area is expected to be especially high.

The input of ^{226}Ra , in the West European Margin, is accompanied by a Ba input since i) positive Ba anomalies are also observed in the deep waters and ii) the $^{226}\text{Ra}/\text{Ba}$ ratios do not significantly deviate from the mean GEOSECS $^{226}\text{Ra}/\text{Ba}$ ratio (Fig.8a). One exception is found at station 21 in the West European Basin, which displays high $^{226}\text{Ra}/\text{Ba}$ at approximately 4000 m (up to $3.17 \text{ dpm } \mu\text{mol}^{-1}$). At several stations (21, 26, 32, 38, 44, 60, 64 and 77), lower beam transmission values near the seafloor indicate presence of suspended sediments likely associated with a nepheloid layer. Nepheloid layers are turbid layers formed episodically by strong and intense abyssal currents that are transported along isopycnals away from the site of resuspension of bottom sediments (McCave, 1986). The presence of a benthic nepheloid layer is also indicated by high particulate iron concentrations at these stations (Gourain et al., 2017; this issue). Such process may thus contribute to release ^{226}Ra (and potentially Ba) to the deep water column, following desorption or dissolution of the particles. Similar ^{226}Ra maxima have been observed in the deep waters of the Northeast Pacific suggesting that the ^{226}Ra flux is not uniform over the ocean bottom even on a regional scale (Chung, 1976).

Positive ^{226}Ra anomalies are also found in deep waters at several other stations located in relatively deep basins ($> 1200 \text{ m}$) along the GA01 section (e.g. stations 32, 38, 44, 60, 64, 69 and 77). Most of these anomalies are associated with $^{226}\text{Ra}/\text{Ba}$ ratios higher than $2.4 \text{ dpm } \mu\text{mol}^{-1}$. The ^{226}Ra positive anomalies observed at the stations mentioned above are thus best explained by the diffusion of ^{226}Ra from the sediment. However, these latter stations do not exhibit a positive Ba anomaly and Ba tends to be conservative. Consequently, the $^{226}\text{Ra}/\text{Ba}$ ratios in the deep waters of these stations are often significantly higher than the mean GEOSECS value (stations 21, 32, 38, 60, 64; Fig.8). This pattern is different to that observed in the West European Basin, a discrepancy that may be explained by the different sediment composition in the two regions and/or by the different residence time of deep waters in contact with deep-sea sediments.

A strong ^{226}Ra positive anomaly is observed in the deepest sample collected at station 38 above the Reykjanes Ridge. It cannot be completely excluded that this positive anomaly is attributed to hydrothermal vent since hydrothermal systems are known in the area (Fig.1). High particulate iron and aluminum concentrations were also observed at these stations (Gourain et al., 2017; Menzel et al., 2017; this issue). Enrichment in ^{226}Ra have indeed been observed in hydrothermal systems plume at mid-ocean Ridges (Kadko, 1996; Kadko and Moore, 1988; Kipp et al., 2017; Rudnicki and Elderfield, 1992). Moreover, the ^{226}Ra enrichments are accompanied by slight Ba enrichments, which may support



the hydrothermal origin hypothesis, since hydrothermal venting at mid-ocean Ridge constitutes the second major external source of Ba to the ocean (Edmond et al., 1979).

Finally, positive ^{226}Ra and Ba anomalies are also observed in shallow coastal waters (Fig.8c). The positive ^{226}Ra anomalies are found close to the bottom, in agreement with the input of ^{226}Ra from the sediment (station 61), whereas the positive Ba anomalies are found in the subsurface (stations 57, 61 and 78) in association with low salinities (Fig.S2). The positive Ba anomalies are thus explained by the input of meteoritic waters in coastal areas, as such waters are known to be the predominant source of Ba to the ocean (Martin and Meybeck, 1979; Wolgemuth and Broecker, 1970). In these shallow stations (140 m-550 m), the different source terms between ^{226}Ra and Ba therefore leads to lower $^{226}\text{Ra}/\text{Ba}$ ratios (Fig.8c.; stations 53, 57, 61 and 78). In contrast, the input of ^{226}Ra from sediment leads to higher $^{226}\text{Ra}/\text{Ba}$ ratios near the seafloor (stations 53 and 61). These observations clearly indicate that ^{226}Ra may sometimes be decoupled from Ba.

4.3.2. ^{226}Ra removal its relationship with Ba

Very few ^{226}Ra negative anomalies were found along the GA01 section. In the deep open-ocean stations, they are mostly observed in the upper 1000 m (Fig.8; stations 38, 44 and 77), but can also be found as deep as 2000 m (i.e., stations 64 and 69). In most cases, the negative ^{226}Ra anomalies are associated with significant negative Ba anomalies (stations 32, 44, 60 and 69). Such features are likely explained by biological mediated processes including incorporation of ^{226}Ra and Ba in planktonic siliceous shells (Bishop, 1988), in acantharian skeletons made of celestite (SrSO_4) or in barite (BaSO_4) crystals (van Beek et al., 2007; Chow and Goldberg, 1960; Shannon and Cherry, 1971; Szabo, 1967; Wolgemuth and Broecker, 1970).

Particularly low dissolved $^{226}\text{Ra}/\text{Ba}$ ratios ($<2 \text{ dpm } \mu\text{mol}^{-1}$) are found in the upper 50 m at stations 21, 32, 64, 69 and 77, a pattern that was also observed in the upper 150 m of the Sargasso Sea, where (van Beek et al., 2007) reported high $^{226}\text{Ra}/\text{Ba}$ in suspended particles attributed to the incorporation of ^{226}Ra and Ba in acantharian skeletons. The low dissolved $^{226}\text{Ra}/\text{Ba}$ ratios (e.g. $1.7 \text{ dpm } \mu\text{mol}^{-1}$, station 77) observed in the upper 200 m along the GA01 section may thus be attributed to acantharians, which have skeletons that incorporate ^{226}Ra preferentially to Ba (van Beek et al., 2007, 2009; Bernstein et al., 1998). Previous studies reported the presence of these organisms in the North Atlantic, especially in the Iceland Basin and in the East Greenland Sea (Antia et al., 1993; Barnard et al., 2004; Martin et al., 2010).

Several phytoplankton blooms were observed along the GA01 section, as indicated by the chlorophyll a concentrations (Chl-a) (Fig.SI2). The largest bloom was observed in the Labrador Sea in May 2014. Since diatoms are the dominant species in the Irminger and Labrador Seas and on the Greenland and Newfoundland margins during GA01 (up to 55 % of the total Chl-a concentration; Tonnard et al., in prep), the diatom frustules may also contribute to the removal of ^{226}Ra and Ba from



the water column in these areas that were characterized by noticeable negative anomalies. In contrast, Chl-a was lower in May and June 2014 in the West European Basin and coccolithophorids were the dominant species in that area. These two observations may thus explain why the ^{226}Ra and Ba removal was less intense in that latter basin.

5 Additionally, because the Labrador Sea was sampled in June, during the decline of the bloom, barite that is presumably formed following the decay of settling organic matter may also contribute to the removal of Ba (and ^{226}Ra). High particulate excess Ba (Ba_{xs}) concentrations were indeed observed at stations displaying significant Ba negative anomalies: Ba_{xs} concentrations reached a maximum at 400 m at station 13 and between 400 and 800 m near Greenland, at stations 44, 64 and 69 (Lemaitre et al.,
10 2017, *Ba paper*, this issue). These Ba_{xs} profiles can be related to the relatively high particulate organic carbon (POC) export flux determined at these stations (eg. at station 69, Lemaitre et al., 2017, *Export paper*; this issue). This POC flux would promote barite formation in subsurface (Dehairs et al., 1980; Legeleux and Reyss, 1996) but also deeper in the water column (van Beek et al., 2007), thus leading to the “biologically” mediated removal of ^{226}Ra . Similarly, (Jullion et al., 2017) – by using a parametric
15 OMP analyses as applied in the Mediterranean Sea – also reported quantification of the non-conservative component of the Ba signal and suggested that the Ba negative anomalies potentially reflected Ba subtraction during barite formation occurring during POC remineralization. The winter deep convection in the Labrador Sea may also potentially explain this relatively deep Ba anomalies by transporting negative Ba and ^{226}Ra anomalies waters toward the deep-sea (Jullion et al., 2017). With the
20 exception of the acantharian skeletons that may impact the dissolved $^{226}\text{Ra}/\text{Ba}$ ratios in the upper 200 m, the removal of ^{226}Ra and Ba that takes place deeper in the water column or that involves other processes (e.g. barite precipitation) does not seem to affect significantly the dissolved $^{226}\text{Ra}/\text{Ba}$ ratios.

In the shallow coastal stations, lower $^{226}\text{Ra}/\text{Ba}$ ratios are observed (Fig.8). These low ratios may also result from the removal of ^{226}Ra and Ba by planktonic shells and/or barite or scavenging onto
25 lithogenic particles. However, because these stations are coastal stations, various processes are at play in a relatively shallow water column (i.e. diffusion of ^{226}Ra from the sediments; input of Ba from meteoritic water; removal of Ba and ^{226}Ra by shells and barite) thus complicating the interpretation of the vertical profiles. We note that the low $^{226}\text{Ra}/\text{Ba}$ ratios observed in surface of shallow stations near the coast of Greenland (stations 57 and 61) and Newfoundland (station 78) are associated with low
30 salinities (Fig.8c). This decoupling between ^{226}Ra and Ba may be explained by input of freshwater into the coastal zone.

Finally, at several stations, a decrease in the ^{226}Ra activities is observed near the seafloor (stations 13, 21, 44, 60, 64 and 77; Fig.8). Similar decreasing trends near the seafloor have been reported in the Southwest Atlantic and North Pacific for ^{230}Th (Deng et al., 2014; Okubo et al., 2012), a
35 reactive element that strongly adsorbs onto suspended particles. This trend for ^{230}Th was explained by nuclide scavenging at the seafloor (Deng et al., 2014; Okubo et al., 2012). Radium-226 – although it is



much less particle-reactive than ^{230}Th – may also be scavenged by resuspended particles near the seafloor and may adsorb onto the surfaces of Mn oxides (Moore and Reid, 1973). High particulate TEs concentrations were also observed at stations 26, 38, and 69 and may be related to nepheloid layers that impact the deep water column up to 200–300 m above the seafloor (Gourain et al., 2017; Menzel et al., 2017; this issue).

4.4. Estimation of ^{226}Ra and Ba input fluxes into the West European Basin

A strong positive anomaly is observed in the NEADWI between stations 1 and 21 and below 3500 m. On average, it is 3.3 dpm 100 L^{-1} over this vertical section. This anomaly reflects a concentration difference between the ^{226}Ra measured along GA01 and the ^{226}Ra due to the water mass mixing. This concentration difference is associated to the northward transport of the NEADWI, estimated to be $0.9 \pm 0.3\text{ Sv}$ ($10^6\text{ m}^3\text{ s}^{-1}$) at 45°N (GA01 section) (Daniault et al., 2016; McCartney, 1992). Therefore, the concentration anomaly can be converted into a ^{226}Ra flux that can be calculated as follows:

$$F_{\text{INPUT}} = A \times T_{\text{NEADWI}} \quad (1)$$

where A is the mean positive anomaly of ^{226}Ra (in dpm m^{-3}) determined by the OMP analysis; T_{NEADWI} is the transport associated with the NEADWI (in $\text{m}^3\text{ s}^{-1}$).

Given that this flux does not result from the mixing of the water masses, the ^{226}Ra flux thus calculated has to reflect an input.

This input may be associated with a sedimentary source. The NEADWI at 45°N is made of up to 92 % of the 11°N NEADWI endmember. Therefore, the sedimentary input along the northward transport of the NEADWI is calculated across a sediment area between 11°N and 45°N (Fig.S2). We consider the distance of 4209 km between 11°N and the GA01 section and the distance of 1475 km between stations 1 and 21. This leads to an area of $6.21 \cdot 10^6\text{ km}^2$ (assuming a constant bathymetry).

The ^{226}Ra flux diffusing out of bottom sediments, F_{sedRa} (in dpm $\text{cm}^{-2}\text{ y}^{-1}$) is calculated using Eq.(2) :

$$F_{\text{sed}} = \frac{F_{\text{INPUT}}}{S} \quad (2)$$

where S is the above described surface area (in cm^2).

The calculated F_{sedRa} is $14.8 \pm 3.1 \cdot 10^{-3}\text{ dpm cm}^{-2}\text{ y}^{-1}$, which is within the range of fluxes reported in the literature. For example, (Cochran, 1980) reported F_{sedRa} in the range of $1.5 \cdot 10^{-3}\text{ dpm cm}^{-2}\text{ y}^{-1}$ for the Atlantic Ocean to $2.1 \cdot 10^{-1}\text{ dpm cm}^{-2}\text{ y}^{-1}$ in the Pacific Ocean (Fig.9). (Li et al., 1973) estimated ^{226}Ra fluxes diffusing out of the sediment in the Southern Ocean and on the Antarctic shelf of $6.2 \cdot 10^{-4}\text{ dpm cm}^{-2}\text{ y}^{-1}$ and $1.6 \cdot 10^{-3}\text{ dpm cm}^{-2}\text{ y}^{-1}$, respectively. The F_{sedRa} calculated here is thus slightly higher than the ^{226}Ra sedimentary fluxes reported in the Atlantic Ocean by Cochran (1980). Note, however, that the ^{226}Ra fluxes released from the sediments vary locally as a function of



the sedimentary ^{230}Th activity, bioturbation rates, but also the sediment type and composition (Chung, 1976; Cochran, 1980). The ^{226}Ra fluxes reported in the Atlantic Ocean by Cochran (1980), which are the lowest of all basins, are only available for calcareous ooze type sediment (Cochran, 1980). The NEADWI may cross different types of sediments along its northward path in the Atlantic Ocean. This includes calcareous oozes, fine-grained calcareous sediments and clay (Dutkiewicz et al., 2015). In particular, ^{226}Ra diffusion is expected to be higher in these two latter sediment types (Cochran, 1980).

As for Ba is concerned, the mean positive anomalies deduced from the OMP analysis is 7.0 nmol L^{-1} . In the same way as ^{226}Ra , a Ba sedimentary flux F_{sedBa} of $3.16 \pm 1.4 \text{ nmol cm}^{-2} \text{ y}^{-1}$ would be required to explain the Ba anomalies in the West European Basin. This flux is on the low end of the Ba sedimentary fluxes reported in different ocean basins, which range from 1.0 to $30 \text{ nmol cm}^{-2} \text{ y}^{-1}$ (Chan et al., 1977; Falkner et al., 1993; McManus et al., 1999; Paytan and Kastner, 1996).

Alternatively, it cannot be excluded that ^{226}Ra and Ba released by settling particles contribute to the ^{226}Ra and Ba anomalies. However, ^{226}Ra activities and Ba concentrations in suspended particles collected in the Atlantic Ocean range from 0.01 and $0.1 \text{ dpm } 100 \text{ L}^{-1}$ and from 0.05 to 0.3 nmol L^{-1} , respectively (van Beek et al., 2007; Dehairs et al., 1980). These latter ^{226}Ra activities and Ba concentrations respectively represent up to 3% and 4% of the mean ^{226}Ra and Ba anomalies ($3.3 \text{ dpm } 100 \text{ L}^{-1}$ and 6.4 nmol L^{-1} , respectively). Therefore, this source does not likely significantly contribute to the positive Ra and Ba anomalies. The ^{226}Ra and Ba positive anomalies observed in the West European Basin are thus best explained by the accumulation of ^{226}Ra and Ba that diffuse out of the sediments.

5. Conclusion

We investigated the distribution of dissolved ^{226}Ra activities and Ba concentrations in the North Atlantic Ocean along the GA01 section. To a first order, the ^{226}Ra and Ba patterns appear to be correlated to the water masses (e.g. high ^{226}Ra and Ba in NEADWI in the West European Basin; low ^{226}Ra and Ba in Central Waters; slight increase of ^{226}Ra in the MW). Using a mixing model, we show that ^{226}Ra and Ba are mostly conservative along the section, with 72% of the ^{226}Ra and 68% of the Ba being conservative. ^{226}Ra and Ba are mostly conservative at intermediate depths (mostly between 500 m and 2000 m) and slightly deeper in the middle of deep basins. These locations correspond to the depths where the waters are away from the main sources of ^{226}Ra and Ba. This indicates that the distributions of ^{226}Ra and Ba at these intermediate depths are largely governed by water mass transport and mixing. The use of the $^{226}\text{Ra}/\text{Ba}$ ratio as a clock to chronometer the thermohaline circulation may thus be relevant when studying water masses at these intermediate depths.

Our study also highlighted several regions where significant input or loss of ^{226}Ra and Ba takes place. In the West European Basin, the deep waters (NEADWI) accumulate both ^{226}Ra and Ba, a pattern that we attribute to the diffusion of ^{226}Ra and Ba out of the sediments, while the waters travel northward



from 11 ° N to the GA01 section. This pattern contrasts with that observed in the deep waters collected elsewhere along the section that do not display Ba enrichment parallel to the ^{226}Ra enrichment. Bottom nepheloid layers may also contribute to the release of ^{226}Ra (and Ba) to the deep water column at several stations. Interestingly, nepheloid layer processes seem to also act as potential removal of ^{226}Ra (and Ba). Significant input of Ba - likely associated with meteoritic waters - is found in the upper water column near Greenland. Finally, ^{226}Ra and Ba are removed from the upper water column, primarily due to biological mediated processes such as incorporation of ^{226}Ra and Ba into barite (BaSO_4) that are presumably formed following the decay of settling organic matter and/or adsorption onto diatom frustules, a mechanism that would explain the ^{226}Ra -Ba-Si relationship reported here .

10 Our study also provides evidence of significant decoupling between ^{226}Ra and Ba. In the upper 200 m, the $^{226}\text{Ra}/\text{Ba}$ ratios reach low values ($<2 \text{ dpm } \mu\text{mol}^{-1}$), a pattern that has been observed in other regions and was related to acantharian skeletons that incorporate ^{226}Ra preferentially to Ba (van Beek et al., 2007; Bernstein et al., 1998). Finally, deviations from the mean GEOSECS $^{226}\text{Ra}/\text{Ba}$ ratios were observed in the shallow coastal waters of Greenland and Newfoundland: the predominant input of Ba
15 due to input of meteoritic waters leads to lower $^{226}\text{Ra}/\text{Ba}$ ratios whereas near the seafloor, the input of sedimentary ^{226}Ra leads to higher $^{226}\text{Ra}/\text{Ba}$ ratios.

The absence of a stable isotope for radium led geochemists to consider Ba as a stable analog for ^{226}Ra because ^{226}Ra and Ba display a similar chemical behavior. This study confirms that ^{226}Ra and Ba behave similarly, both elements being mostly conservative along the GA01 section, thus ^{226}Ra and Ba
20 can be considered as conservative tracers in the ocean interior. However, this study also highlights regions where ^{226}Ra and Ba deviate from conservative mixing, an important consideration when considering the balance between the large-scale oceanic circulation and biological activity over long time scales. Decoupling between ^{226}Ra and Ba has been observed, in most cases at the ocean boundaries. We are hopeful that these new constraints on oceanic ^{226}Ra and Ba distributions will help to
25 refine the use of the $^{226}\text{Ra}/\text{Ba}$ ratio as a clock to chronometer the thermohaline circulation, as was proposed several decades ago during the GEOSECS program.



Figure Caption

- Figure 1:** Station locations of the GA01 section between Portugal and Newfoundland in the North Atlantic (black and blue dots). Stations investigated for ^{226}Ra and Ba are marked as blue dots. The main currents and water masses in the North Atlantic are also represented. The major hydrothermal vents located near the GA01 section are indicated by black triangles. Stations investigated during the US-GEOTRACES-GA03 section, also conducted in the Atlantic Ocean, are reported on the lower panel (red dots).
- Figure 2:** Potential temperature-salinity diagram—including a zoom for bottom waters—of the water samples (colored dots) from the GA01 section. The properties of the source water types (based on García-Ibáñez et al., 2017; This issue) used in the Optimum Multiparameter (OMP) analysis are reported with white circles. Isopycnals are also plotted (potential density referenced to 0 dbar).
- Figure 3:** Distribution of salinity (CTD data) along the GA01 section. The different water masses are also reported, following García-Ibáñez et al. (2017; this issue). The station numbers are found on top of the figure. The sampling depths for ^{226}Ra are shown for each vertical profile (black dots).
- Figure 4:** Distribution of dissolved ^{226}Ra activities ($\text{dpm } 100 \text{ L}^{-1}$) and dissolved Ba concentrations (nmol L^{-1} ; white contour lines) along the GA01 section. Station numbers are found on top of the panel. The sampling depths for ^{226}Ra are shown for each vertical profile (black dots).
- Figure 5:** Relationships between ^{226}Ra and Ba (red dots) and between ^{226}Ra and $\text{Si}(\text{OH})_4$ (blue dots) along the GA01 section in the North Atlantic. The best linear fit for the two plots is also reported ($R=0.93$ for the two plots).
- Figure 6:** Geographical variation of ^{226}Ra activities (red dots), salinity (blue dots), temperature (yellow dots) and $\text{Si}(\text{OH})_4$ concentrations (green dots) in AABW between 60°S and 45°N (GA01 section) in the Atlantic Ocean based on data from the GEOSECS and TTO programs. The ^{226}Ra activities, salinity, temperature and $\text{Si}(\text{OH})_4$ concentrations from GA01 are represented with open circles. The values used as endmembers for the OMP analysis are also identified by the black circles. The shaded area represents the region where transformation of the AABW into NEADW takes place.
- Figure 7:** Difference between the measured concentrations and those calculated by the OMP analysis, for ^{226}Ra (a) and Ba (b) along the GA01 section. Positive anomalies reflect recent tracer addition, while negative ones reflect recent tracer removal. Station numbers are found on top of both panels.
- Figure 8:** Vertical profiles of dissolved ^{226}Ra activities and Ba concentrations determined along the GA01 section: (a) West European Basin; (b) Iceland Basin and Irminger Sea, (c) the Greenland and Newfoundland margins, and (d) Labrador Sea. As a comparison, the conservative ^{226}Ra and Ba vertical profiles derived from the OMP analysis are also reported in solid grey lines. The discrepancy between the two vertical profiles indicates deviation from the conservative behavior and reflects either an input of ^{226}Ra or Ba (positive anomalies highlighted in red; same color code as Fig.8) or a removal of ^{226}Ra or Ba (negative anomalies highlighted in blue; same color code as Fig.8). The OMP analysis has not been solved for the shallow coastal stations 53 and 78. The $^{226}\text{Ra}/\text{Ba}$ ratios are also reported, together with the mean GEOSECS $^{226}\text{Ra}/\text{Ba}$ ratio ($2.2 \pm 0.2 \text{ dpm } \mu\text{mol}^{-1}$; black dashed line) together with its one standard deviation (grey shaded areas). Note that the scale may be different from one station to the other and the vertical axis was cut to 1000 m. The seafloor is represented by the bottom axis.
- Figure 9:** ^{226}Ra fluxes diffusing out of the sediment in relationship with bottom water ^{226}Ra activities determined in different oceanic basins (P=Pacific Ocean, A=Atlantic Ocean, I=Indian Ocean and AA=Southern Ocean) by Cochran (1980). The ^{226}Ra flux calculated in this study to explain the positive anomalies in the West European Basin is also reported (red dot).



Acknowledgement

The present research and Emilie Le Roy's fellowship are co-funded by the European Union and the Région Occitanie-Pyrénées-Méditerranée (European Regional Development Fund). We are grateful to the captain and crew of the N/O *Pourquoi Pas?*. The GEOVIDE project is co-funded by the French national program LEFE/INSU (GEOVIDE), ANR Blanc (GEOVIDE, ANR-13-BS06-0014) and RPDOC (ANR-12-PDOC-0025-01), LabEX MER (ANR-10-LABX-19) and IFREMER. The GEOVIDE cruise would not have been achieved without the technical skills and commitment of Catherine Kermabon, Olivier Ménage, Stéphane Leizour, Michel Hamon, Philippe Le Bot, Emmanuel de Saint-Léger and Fabien Pérault. We are grateful to Manon Le Goff, Emilie Grosstefan, Morgane Gallinari and Paul Tréguer for $\text{Si}(\text{OH})_4$ sampling and analysis. This work was also co-funded by the French national program LEFE/INSU "REPAP" (PI S. Jacquet) and the U.S. National Science Foundation (PI M. Charette, OCE- 1458305; OCE- 1232669). For this work M.I. García-Ibáñez and F.F. Pérez were supported by the Spanish Ministry of Economy and Competitiveness through the BOCATS (CTM2013-41048-P) project co-funded by the Fondo Europeo de Desarrollo Regional 2014–2020 (FEDER). Several figures were constructed using Ocean Data View (Schlitzer, 2003). Therefore, R. Schlitzer is warmly thanked. Satellite chlorophyll-a visualizations used in this study were produced with the Giovanni online data system, developed and maintained by the NASA GES DISC.

References

- Antia, A. N., Bauerfeind, E., Bodungen, B. v and Zeller, U.: Abundance, encystment and sedimentation of acantharia during autumn 1990 in the East Greenland Sea, *J. Plankton Res.*, 15(1), 99–114, doi:10.1093/plankt/15.1.99, 1993.
- Bacon, M. P. and Anderson, R. F.: Distribution of thorium isotopes between dissolved and particulate forms in the deep sea, *J. Geophys. Res. Oceans*, 87(C3), 2045–2056, doi:10.1029/JC087iC03p02045, 1982.
- Barnard, R. T., Batten, S., Beaugrand, G., Buckland, C., Conway, D. V. P., Edwards, M., Finlayson, J., Gregory, L. W., Halliday, N. C., John, A. W. G., Johns, D. G., Johnson, A. D., Jonas, T. D., Lindley, J. A., Nyman, J., Pritchard, P., Reid, P. C., Richardson, A. J., Saxby, R. E., Sidey, J., Smith, M. A., Stevens, D. P., Taylor, C. M., Tranter, P. R. G., Walne, A. W., Wootton, M., Wotton, C. O. M. and Wright, J. C.: Continuous plankton records: Plankton atlas of the North Atlantic Ocean (1958-1999). II. Biogeographical charts, *Mar. Ecol.-Prog. Ser.*, MEPS supplement(SUPPL.), 11–75, 2004.
- Bennett, T., Broecker, W. S. and Hansen, J.: North Atlantic Deep Water Formation, 1985.
- Bernstein, R. E., Byrne, R. H. and Schijf, J.: Acantharians: a missing link in the oceanic biogeochemistry of barium, *Deep Sea Res. Part Oceanogr. Res. Pap.*, 45(2), 491–505, doi:10.1016/S0967-0637(97)00095-2, 1998.
- Bishop, J. K. B.: The barite-opal-organic carbon association in oceanic particulate matter, *Nature*, 332(6162), 341–343, doi:10.1038/332341a0, 1988.



- Broecker, W., Kaufman, A., Ku, T.-L., Chung, Y.-C. and Craig, H.: Radium 226 measurements from the 1969 North Pacific Geosecs Station, *J. Geophys. Res.*, 75(36), 7682–7685, doi:10.1029/JC075i036p07682, 1970.
- Broecker, W. S., Li, Y.-H. and Cromwell, J.: Radium-226 and Radon-222 : Concentration in Atlantic and Pacific Oceans, *Science*, 158(3806), 1307–1310, 1967.
- Broecker, W. S., Goddard, J. and Sarmiento, J. L.: The distribution of 226Ra in the Atlantic Ocean, *Earth Planet. Sci. Lett.*, 32(2), 220–235, doi:10.1016/0012-821X(76)90063-7, 1976.
- Chan, L. H., Edmond, J. M., Stallard, R. F., Broecker, W. S., Chung, Y. C., Weiss, R. F. and Ku, T. L.: Radium and barium at GEOSECS stations in the Atlantic and Pacific, *Earth Planet. Sci. Lett.*, 32(2), 258–267, 1976.
- Chan, L. H., Drummond, D., Edmond, J. M. and Grant, B.: On the barium data from the Atlantic GEOSECS expedition, *Deep Sea Res.*, 24(7), 613–649, doi:10.1016/0146-6291(77)90505-7, 1977.
- Charette, M. A., Morris, P. J., Henderson, P. B. and Moore, W. S.: Radium isotope distributions during the US GEOTRACES North Atlantic cruises, *Mar. Chem.*, 177, Part 1, 184–195, doi:10.1016/j.marchem.2015.01.001, 2015.
- Chow, T. J. and Goldberg, E. D.: On the marine geochemistry of barium, *Geochim. Cosmochim. Acta*, 20(3), 192–198, doi:10.1016/0016-7037(60)90073-9, 1960.
- Chung, Y.: Radium-barium-silica correlations and a two-dimensional radium model for the world ocean, *Earth Planet. Sci. Lett.*, 49(2), 309–318, doi:10.1016/0012-821X(80)90074-6, 1980.
- Chung, Y., Craig, H., Ku, T. L., Goddard, J. and Broecker, W. S.: Radium-226 measurements from three Geosecs intercalibration stations, *Earth Planet. Sci. Lett.*, 23(1), 116–124, doi:10.1016/0012-821X(74)90038-7, 1974.
- Chung, Y.-C.: A deep 226Ra maximum in the Northeast Pacific, *Earth Planet. Sci. Lett.*, 32, 249–257, doi:10.1016/0012-821X(76)90065-0, 1976.
- Chung, Y.-C. and Craig, H.: 226Ra in the Pacific Ocean, *Earth Planet. Sci. Lett.*, 49, 267–292, 1980.
- Cochran, J. K.: The flux of 226Ra from deep-sea sediments, *Earth Planet. Sci. Lett.*, 49(2), 381–392, doi:10.1016/0012-821X(80)90080-1, 1980.
- Cochran, J. K. and Krishnaswami, S.: Radium, thorium, uranium, and 210 Pb in deep-sea sediments and sediment pore waters from the North Equatorial Pacific, *Am. J. Sci.*, 280, 849–889, doi:10.2475/ajs.280.9.849, 1980.
- Daniault, N., Lherminier, P. and Mercier, H.: Circulation and Transport at the Southeast Tip of Greenland, *J. Phys. Oceanogr.*, 41(3), 437–457, doi:10.1175/2010JPO4428.1, 2011.
- Daniault, N., Mercier, H., Lherminier, P., Sarafanov, A., Falina, A., Zunino, P., Pérez, F. F., Ríos, A. F., Ferron, B., Huck, T., Thierry, V. and Gladyshev, S.: The northern North Atlantic Ocean mean circulation in the early 21st century, *Prog. Oceanogr.*, 146, 142–158, doi:10.1016/j.pocean.2016.06.007, 2016.
- Dehairs, F., Chesselet, R. and Jedwab, J.: Discrete suspended particles of barite and the barium cycle in the open ocean, *Earth Planet. Sci. Lett.*, 49(2), 528–550, doi:10.1016/0012-821X(80)90094-1, 1980.



- Deng, F., Thomas, A. L., Rijkenberg, M. J. A. and Henderson, G. M.: Controls on seawater ²³¹Pa, ²³⁰Th and ²³²Th concentrations along the flow paths of deep waters in the Southwest Atlantic, *Earth Planet. Sci. Lett.*, 390, 93–102, doi:10.1016/j.epsl.2013.12.038, 2014.
- Dileep Kumar, M. and Li, Y.-H.: Spreading of water masses and regeneration of silica and ²²⁶Ra in the Indian Ocean, *Deep Sea Res. Part II Top. Stud. Oceanogr.*, 43(1), 83–110, doi:10.1016/0967-0645(95)00084-4, 1996.
- Dutkiewicz, A., Müller, R. D., O’Callaghan, S. and Jónasson, H.: Census of seafloor sediments in the world’s ocean, *Geology*, 43(9), 795–798, doi:10.1130/G36883.1, 2015.
- Edmond, J. M., Measures, C., McDuff, R. E., Chan, L. H., Collier, R., Grant, B., Gordon, L. I. and Corliss, J. B.: Ridge crest hydrothermal activity and the balances of the major and minor elements in the ocean: The Galapagos data, *Earth Planet. Sci. Lett.*, 46(1), 1–18, doi:10.1016/0012-821X(79)90061-X, 1979.
- Falina, A., Sarafanov, A., Mercier, H., Lherminier, P., Sokov, A. and Danialt, N.: On the Cascading of Dense Shelf Waters in the Irminger Sea, *J. Phys. Oceanogr.*, 42(12), 2254–2267, doi:10.1175/JPO-D-12-012.1, 2012.
- Falkner, K. K., klinkhammer, G. P., Bowers, T. S., Todd, J. F., Lewis, B. L., Landing, W. M. and Edmond, J. M.: The behavior of barium in anoxic marine waters, *Geochim. Cosmochim. Acta*, 57(3), 537–554, doi:10.1016/0016-7037(93)90366-5, 1993.
- Fanning, K. A., Vargo, G. A., Bell-Torres, L. and Young, R. W.: Covariation of reactive solutes in the sea, *Mar. Chem.*, 24(3-4), 215–238, 1988.
- Foster, D. A., Staubwasser, M. and Henderson, G. M.: ²²⁶Ra and Ba concentrations in the Ross Sea measured with multicollector ICP mass spectrometry, *Mar. Chem.*, 87(1-2), 59–71, 2004.
- Freydier, R., Dupre, B. and Polve, M.: Analyses by inductively coupled plasma mass spectrometry of Ba concentrations in water and rock samples. Comparison between isotope dilution and external calibration with or without internal standard, *Eur. J. Mass Spectrom.*, 1(3), 283–291, doi:10.1255/ejms.140, 1995.
- Fröb, F., Olsen, A., Våge, K., Moore, G. W. K., Yashayaev, I., Jeansson, E. and Rajasakaren, B.: Irminger Sea deep convection injects oxygen and anthropogenic carbon to the ocean interior, *Nat. Commun.*, 7, ncomms13244, doi:10.1038/ncomms13244, 2016.
- García-Ibáñez, M. I., Pardo, P. C., Carracedo, L. I., Mercier, H., Lherminier, P., Ríos, A. F. and Pérez, F. F.: Structure, transports and transformations of the water masses in the Atlantic Subpolar Gyre, *Prog. Oceanogr.*, 135, 18–36, doi:10.1016/j.pocean.2015.03.009, 2015.
- Henderson, P., Morris, P., Moore, W. and Charette, M.: Methodological advances for measuring low-level radium isotopes in seawater, *J. Radioanal. Nucl. Chem.*, 296(1), 357–362, doi:10.1007/s10967-012-2047-9, 2013.
- Jacquet, S. H. M., Dehairs, F., Cardinal, D., Navez, J. and Delille, B.: Barium distribution across the Southern Ocean frontal system in the Crozet–Kerguelen Basin, *Mar. Chem.*, 95(3–4), 149–162, doi:10.1016/j.marchem.2004.09.002, 2005.
- Jacquet, S. H. M., Dehairs, F., Elskens, M., Savoye, N. and Cardinal, D.: Barium cycling along WOCE SR3 line in the Southern Ocean, *Mar. Chem.*, (1-2) [online] Available from: <http://vliz.be/en/imis?module=ref&refid=211233&basketaction=add> (Accessed 20 January 2017), 2007.



- Jeandel, C., Dupré, B., Lebaron, G., Monnin, C. and Minster, J.-F.: Longitudinal distributions of dissolved barium, silica and alkalinity in the western and southern Indian Ocean, *Deep Sea Res. Part Oceanogr. Res.*, 43, 1–31, doi:10.1016/0967-0637(95)00098-4, 1996.
- Jenkins, W. J., Smethie Jr., W. M., Boyle, E. A. and Cutter, G. A.: Water mass analysis for the U.S. GEOTRACES (GA03) North Atlantic sections, *Deep Sea Res. Part II Top. Stud. Oceanogr.*, 116, 6–20, doi:10.1016/j.dsr2.2014.11.018, 2015.
- Jullion, L., Jacquet, S. H. M. and Tanhua, T.: Untangling biogeochemical processes from the impact of ocean circulation: First insight on the Mediterranean dissolved barium dynamics, *Glob. Biogeochem. Cycles*, 2016GB005489, doi:10.1002/2016GB005489, 2017.
- 10 Kadko, D.: Radioisotopic studies of submarine hydrothermal vents, *Rev. Geophys.*, 34(3), 349–366, doi:10.1029/96RG01762, 1996.
- Kadko, D. and Moore, W.: Radiochemical constraints on the crustal residence time of submarine hydrothermal fluids: Endeavour Ridge, *Geochim. Cosmochim. Acta*, 52(3), 659–668, doi:10.1016/0016-7037(88)90328-6, 1988.
- 15 Key, R. M., Guinasso, N. L. and Schink, D. R.: Emanation of radon-222 from marine sediments, *Mar. Chem.*, 7(3), 221–250, doi:10.1016/0304-4203(79)90041-0, 1979.
- Kipp, L. E., Sanial, V., Henderson, P. B., van Beek, P., Reyss, J.-L., Hammond, D. E., Moore, W. S. and Charette, M. A.: Radium isotopes as tracers of hydrothermal inputs and neutrally buoyant plume dynamics in the deep ocean, *Mar. Chem.*, doi:10.1016/j.marchem.2017.06.011, 2017.
- 20 Klinkhammer, G. P. and Chan, L. H.: Determination of barium in marine waters by isotope dilution inductively coupled plasma mass spectrometry, *Anal. Chim. Acta*, 232, doi:10.1016/s0003-2670(00)81249-0, 1990.
- Koczy, F. F.: Natural radium as a tracer in the ocean, , 18, 351–357, 1958.
- Krauss, W.: Currents and mixing in the Irminger Sea and in the Iceland Basin, *J. Geophys. Res. Oceans*, 25 100(C6), 10851–10871, doi:10.1029/95JC00423, 1995.
- Kröll, V.: Vertical Distribution of Radium in Deep-Sea Sediments, *Nature*, 171(4356), 742–742, doi:10.1038/171742a0, 1953.
- Ku, T.-L. and Lin, M.-C.: ²²⁶Ra distribution in the Antarctic Ocean, *Earth Planet. Sci. Lett.*, 32(2), 236–248, doi:10.1016/0012-821X(76)90064-9, 1976.
- 30 Ku, T.-L. and Luo, S.: New appraisal of radium 226 as a large-scale oceanic mixing tracer, *J. Geophys. Res. Oceans*, 99(C5), 10255–10273, doi:10.1029/94JC00089, 1994.
- Ku, T. L., Li, Y. H., Mathieu, G. G. and Wong, H. K.: Radium in the Indian-Antarctic Ocean south of Australia, *J. Geophys. Res.*, 75(27), 5286–5292, doi:10.1029/JC075i027p05286, 1970.
- 35 Ku, T. L., Huh, C. A. and Chen, P. S.: Meridional distribution of ²²⁶Ra in the eastern Pacific along GEOSECS cruise tracks, *Earth Planet. Sci. Lett.*, 49, 293–308, doi:10.1016/0012-821X(80)90073-4, 1980.
- Lacan, F. and Jeandel, C.: Denmark Strait water circulation traced by heterogeneity in neodymium isotopic compositions, *Deep Sea Res. Part Oceanogr. Res. Pap.*, 51(1), 71–82, 2004.
- Lazier, J. R. N.: The renewal of Labrador sea water, *Deep Sea Res. Oceanogr. Abstr.*, 20(4), 341–353, 40 doi:10.1016/0011-7471(73)90058-2, 1973.



- Legeleux, F. and Reys, J.-L.: $^{228}\text{Ra}/^{226}\text{Ra}$ activity ratio in oceanic settling particles: implications regarding the use of barium as a proxy for paleoproductivity reconstruction, *Deep Sea Res. Part Oceanogr. Res. Pap.*, 43(11), 1857–1863, doi:10.1016/S0967-0637(96)00086-6, 1996.
- Lherminier, P., Mercier, H., Huck, T., Gourcuff, C., Perez, F. F., Morin, P., Sarafanov, A. and Falina, A.: The Atlantic Meridional Overturning Circulation and the subpolar gyre observed at the A25-OVIDE section in June 2002 and 2004, *Deep Sea Res. Part Oceanogr. Res. Pap.*, 57(11), 1374–1391, doi:10.1016/j.dsr.2010.07.009, 2010.
- Li, Y. H., Ku, T. L., Mathieu, G. G. and Wolgemuth, K.: Barium in the Antarctic Ocean and implications regarding the marine geochemistry of Ba and ^{226}Ra , *Earth Planet. Sci. Lett.*, 19(3), 352–358, doi:10.1016/0012-821X(73)90085-X, 1973.
- Lucas, H. F.: Improved Low-Level Alpha-Scintillation Counter for Radon, *Rev. Sci. Instrum.*, 28(9), 680, doi:10.1063/1.1715975, 1957.
- Martin, J.-M. and Meybeck, M.: Elemental mass-balance of material carried by major world rivers, *Mar. Chem.*, 7(3), 173–206, doi:10.1016/0304-4203(79)90039-2, 1979.
- 15 Martin, P., Allen, J. T., Cooper, M. J., Johns, D. G., Lampitt, R. S., Sanders, R. and Teagle, D. A. H.: Sedimentation of acantharian cysts in the Iceland Basin: Strontium as a ballast for deep ocean particle flux, and implications for acantharian reproductive strategies, *Limnol. Oceanogr.*, 55(2), 604–614, doi:10.4319/lo.2010.55.2.0604, 2010.
- Mathieu, G. G. and Wolgemuth, K.: Barium in the Antarctic Ocean and Implication regarding the marine geochemistry of Ba and ^{226}Ra , *EARTH Planet. Sci. Lett.*, 19, 352–358, 1973.
- 20 McCartney, M. S.: Recirculating components to the deep boundary current of the northern North Atlantic, *Prog. Oceanogr.*, 29, 283–383, 1992.
- McCave, I. N.: Local and global aspects of the bottom nepheloid layers in the world ocean, *Neth. J. Sea Res.*, 20(2), 167–181, doi:10.1016/0077-7579(86)90040-2, 1986.
- 25 McManus, J., Berelson, W. M., Hammond, D. E. and Klinkhammer, G. P.: Barium Cycling in the North Pacific: Implications for the Utility of Ba as a Paleoproductivity and Paleoalkalinity Proxy, *Paleoceanography*, 14(1), 53–61, doi:10.1029/1998PA900007, 1999.
- Monnin, C., Jeandel, C., Cattaldo, T. and Dehairs, F.: The marine barite saturation state of the world's oceans, *Mar. Chem.*, 65(3), 253–261, doi:10.1016/S0304-4203(99)00016-X, 1999.
- 30 Moore, W. S. and Reid, D. F.: Extraction of radium from natural waters using manganese-impregnated acrylic fibers, *J. Geophys. Res.*, 78(36), 8880–8886, doi:10.1029/JC078i036p08880, 1973.
- Nozaki, Y.: Excess ^{227}Ac in deep ocean water, *Nature*, 310(5977), 486–488, doi:10.1038/310486a0, 1984.
- Okubo, A., Obata, H., Gamo, T. and Yamada, M.: ^{230}Th and ^{232}Th distributions in mid-latitudes of the North Pacific Ocean: Effect of bottom scavenging, *Earth Planet. Sci. Lett.*, 339–340, 139–150, doi:10.1016/j.epsl.2012.05.012, 2012.
- Östlund, H. G., Craig, H. C., Broecker, W. S., Spencer, D. W. and GEOSECS: Shorebased measurements during the GEOSECS Atlantic expedition, , doi:10.1594/PANGAEA.824123, 1987.
- Paytan, A. and Kastner, M.: Benthic Ba fluxes in the central Equatorial Pacific, implications for the oceanic Ba cycle, *Earth Planet. Sci. Lett.*, 142(3), 439–450, doi:10.1016/0012-821X(96)00120-3, 1996.
- 40



- Peterson, R. N., Burnett, W. C., Dimova, N. and Santos, I. R.: Comparison of measurement methods for radium-226 on manganese-fiber, *Limnol. Oceanogr. Methods*, 7(2), 196–205, doi:10.4319/lom.2009.7.196, 2009.
- Pickart, R. S. and Spall, M. A.: Impact of Labrador Sea Convection on the North Atlantic Meridional
5 Overturning Circulation, *J. Phys. Oceanogr.*, 37(9), 2207–2227, doi:10.1175/JPO3178.1, 2007.
- Pickart, R. S., Straneo, F. and Moore, G. W. K.: Is Labrador sea water formed in the Irminger basin?, *Deep Sea Res. Part Oceanogr. Res. Pap.*, 50(1), 23–52, 2003.
- Read, J. F.: CONVEX-91: water masses and circulation of the Northeast Atlantic subpolar gyre, *Prog. Oceanogr.*, 48(4), 461–510, doi:10.1016/S0079-6611(01)00011-8, 2000.
- 10 Rubin, S. I., King, S. L., Jahnke, R. A. and Froelich, P. N.: Benthic barium and alkalinity fluxes: Is Ba an oceanic paleo-alkalinity proxy for glacial atmospheric CO₂?, *Geophys. Res. Lett.*, 30(17), 1885, doi:10.1029/2003GL017339, 2003.
- Rudels, B., Fahrbach, E., Meincke, J., Budéus, G. and Eriksson, P.: The East Greenland Current and its
15 contribution to the Denmark Strait overflow, *ICES J. Mar. Sci.*, 59(6), 1133–1154, doi:10.1006/jmsc.2002.1284, 2002.
- Rudnicki, M. D. and Elderfield, H.: Helium, radon and manganese at the TAG and Snakepit hydrothermal vent fields, 26° and 23°N, Mid-Atlantic Ridge, *Earth Planet. Sci. Lett.*, 113(3), 307–321, doi:10.1016/0012-821X(92)90136-J, 1992.
- Schmidt, S. and Reyss, J.-L.: Radium as internal tracer of Mediterranean Outflow Water, *J. Geophys.*
20 *Res. Oceans*, 101(C2), 3589–3596, doi:10.1029/95JC03308, 1996.
- Schmitz, W. J. and McCartney, M. S.: On the North Atlantic Circulation, *Rev. Geophys.*, 31(1), 29–49, doi:10.1029/92RG02583, 1993.
- Seager, R., Battisti, D. S., Yin, J., Gordon, N., Naik, N., Clement, A. C. and Cane, M. A.: Is the Gulf Stream responsible for Europe's mild winters?, *Q. J. R. Meteorol. Soc.*, 128(586), 2563–2586,
25 doi:10.1256/qj.01.128, 2002.
- Shannon, L. V. and Cherry, R. D.: Radium-226 in marine phytoplankton, *Earth Planet. Sci. Lett.*, 11(1), 339–343, doi:10.1016/0012-821X(71)90189-0, 1971.
- Szabo, B. J.: Radium content in plankton and sea water in the Bahamas, *Geochim. Cosmochim. Acta*, 31(8), 1321–1331, doi:10.1016/S0016-7037(67)80018-8, 1967.
- 30 van Aken, H. M.: The hydrography of the mid-latitude northeast Atlantic Ocean. I: The deep water masses, *Deep-Sea Res. Part I*, 47, 757–788, doi:10.1016/S0967-0637(99)00092-8, 2000.
- van Aken, H. M. and Becker, G.: Hydrography and through-flow in the north-eastern North Atlantic Ocean: the NANSEN project, *Prog. Oceanogr.*, 38(4), 297–346, doi:10.1016/S0079-6611(97)00005-0, 1996.
- 35 van Beek, P., François, R., Conte, M., Reyss, J.-L., Souhaut, M. and Charette, M.: 228Ra/226Ra and 226Ra/Ba ratios to track barite formation and transport in the water column, *Geochim. Cosmochim. Acta*, 71(1), 71–86, doi:10.1016/j.gca.2006.07.041, 2007.
- van Beek, P., Sternberg, E., Reyss, J. L., Souhaut, M., Robin, E. and Jeandel, C.: 228Ra/226Ra and 226Ra/Ba ratios in the Western Mediterranean Sea : barite formation and transport in the water column,
40 *Geochim. Cosmochim. Acta*, 73, 4720–4737, doi:10.1016/j.gca.2009.05.063, 2009.



van Beek, P., Souhaut, M. and Reyss, J.-L.: Measuring the radium quartet (228Ra, 226Ra, 224Ra, 223Ra) in seawater samples using gamma spectrometry, *J. Environ. Radioact.*, 101(7), 521–529, doi:10.1016/j.jenvrad.2009.12.002, 2010.

5 Wolgemuth, K. and Broecker, W. S.: Barium in sea water, *Earth Planet. Sci. Lett.*, 8(5), 372–378, doi:10.1016/0012-821X(70)90110-X, 1970.

Yashayaev, I. and Dickson, B.: Transformation and Fate of Overflows in the Northern North Atlantic, in *Arctic–Subarctic Ocean Fluxes*, edited by R. R. Dickson, J. Meincke, and P. Rhines, pp. 505–526, Springer Netherlands. [online] Available from: http://link.springer.com/chapter/10.1007/978-1-4020-6774-7_22 (Accessed 11 April 2016), 2008.

10 Yashayaev, I. and Loder, J. W.: Recurrent replenishment of Labrador Sea Water and associated decadal-scale variability, *J. Geophys. Res. Oceans*, 121(11), 8095–8114, doi:10.1002/2016JC012046, 2016.

Yashayaev, I., Bersch, M. and van Aken, H. M.: Spreading of the Labrador Sea Water to the Irminger and Iceland basins, *Geophys. Res. Lett.*, 34(10), doi:10.1029/2006GL028999, 2007.

15



Figure 1

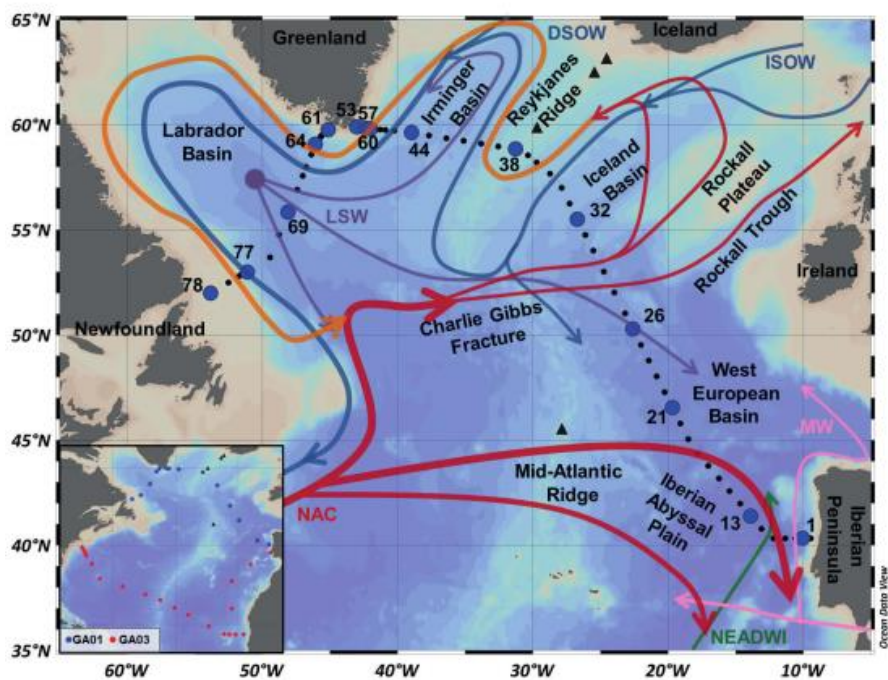




Figure 2

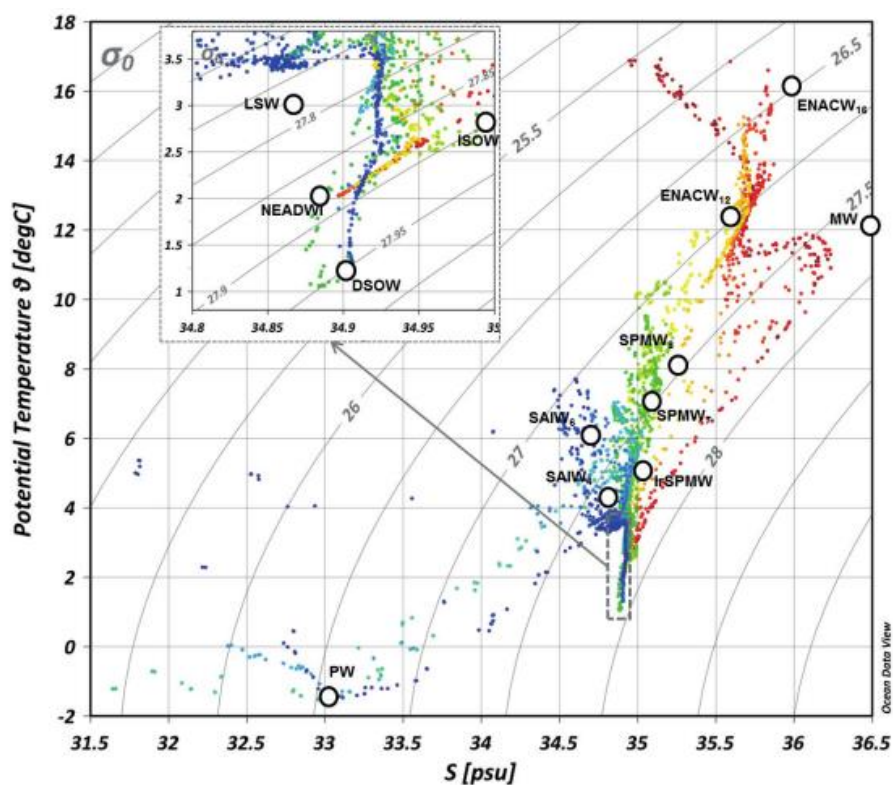




Figure 3

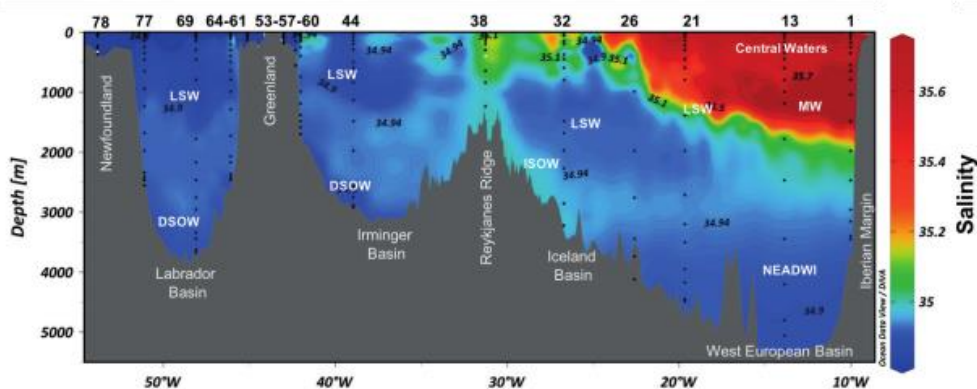




Figure 4

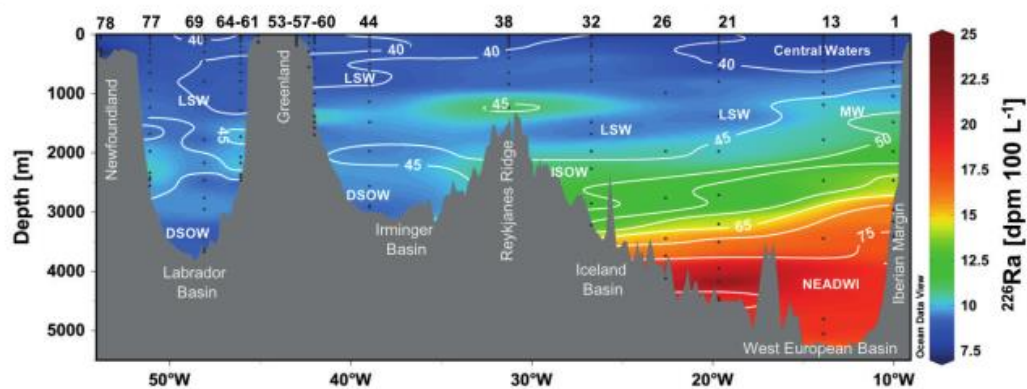




Figure 5

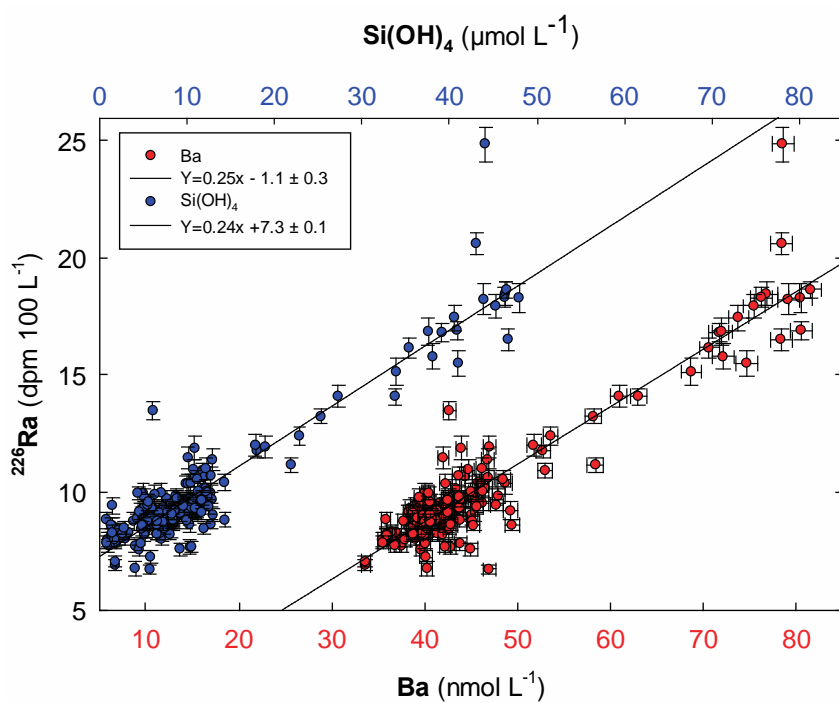




Figure 6

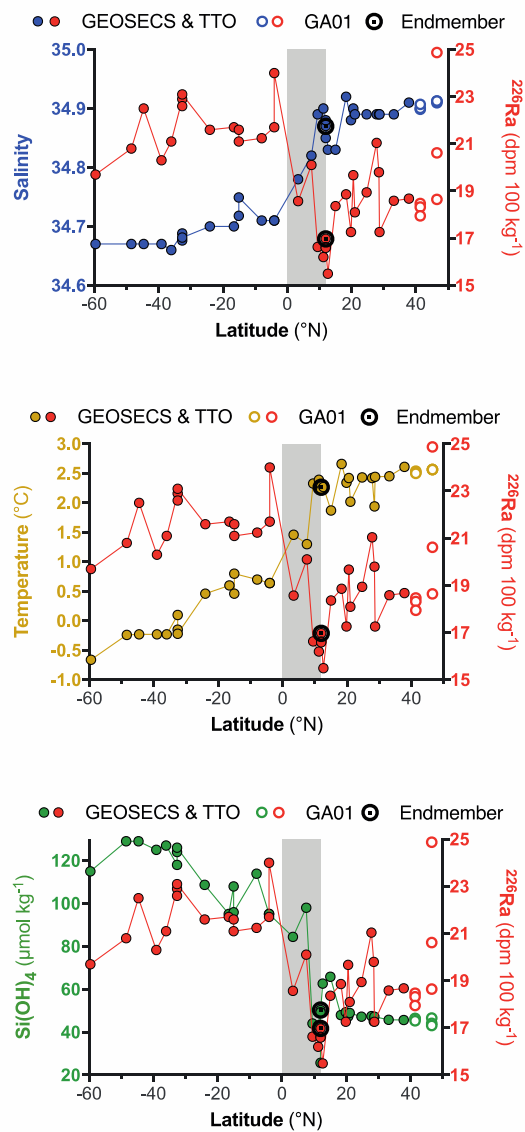




Figure 7

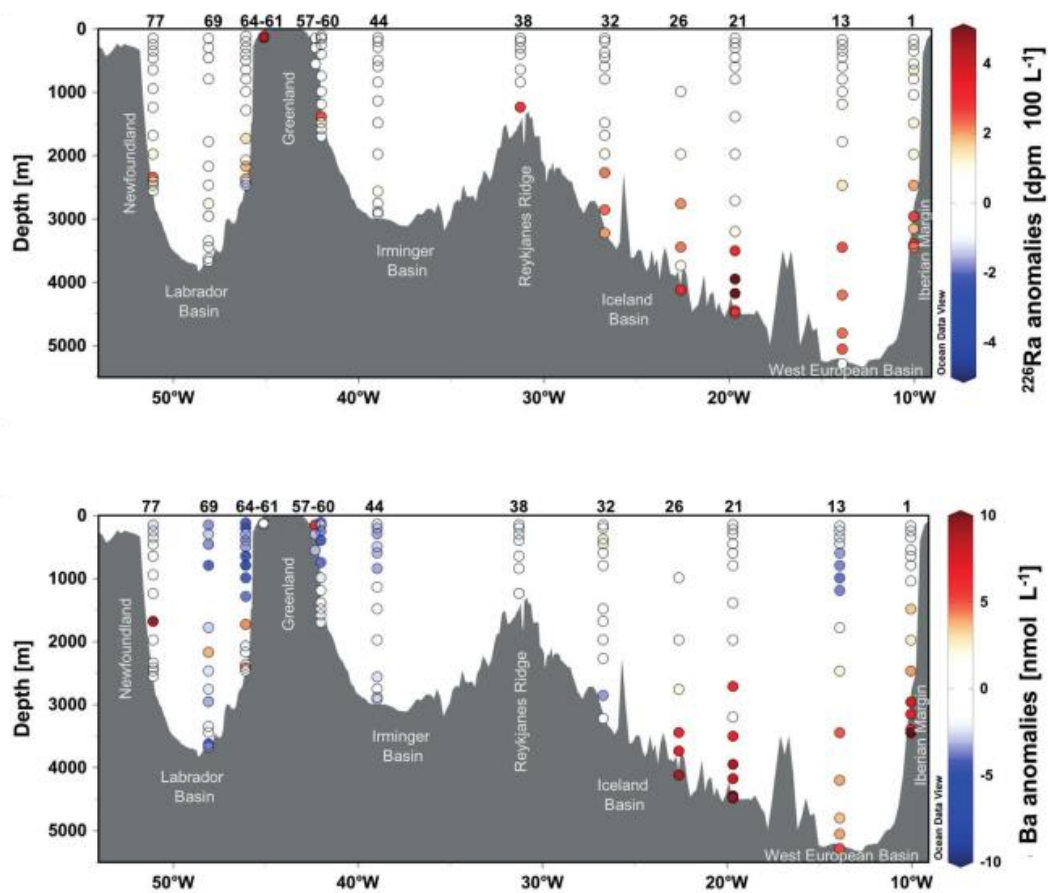
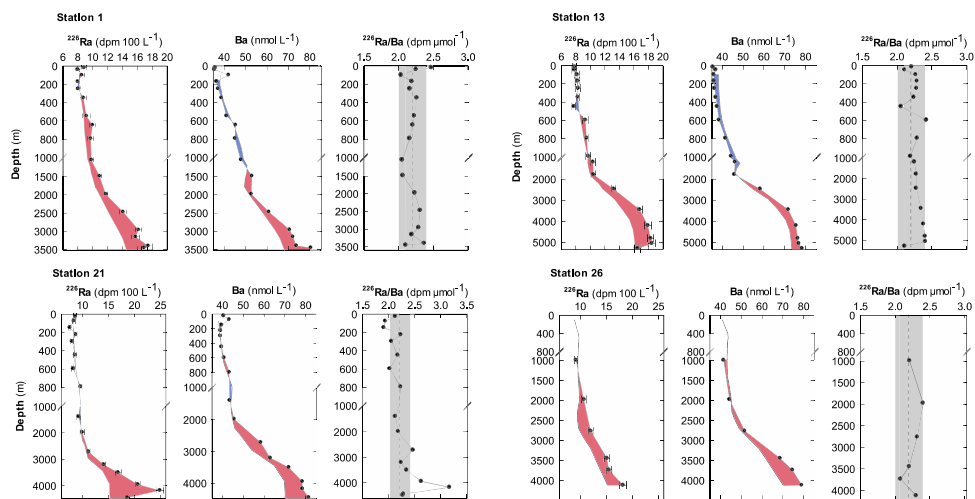




Figure 8

A) West European Basin



B) Iceland and Irminger Basins

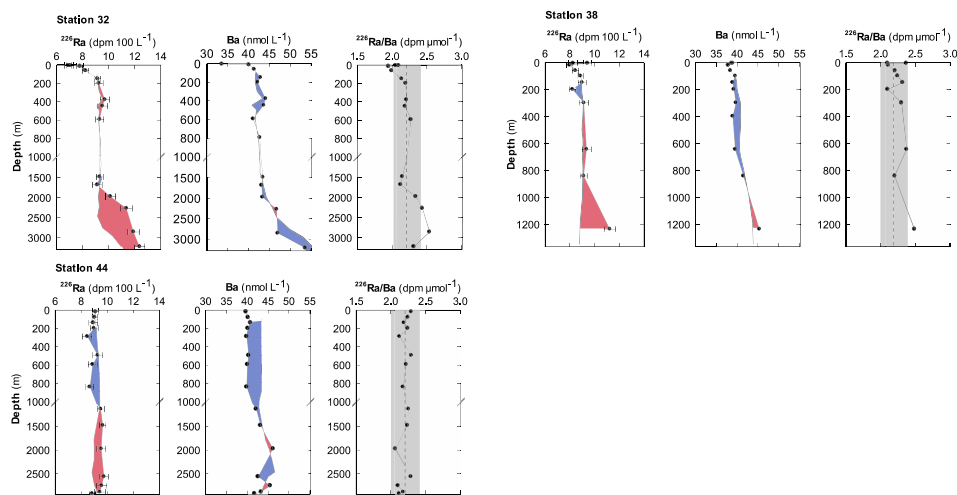
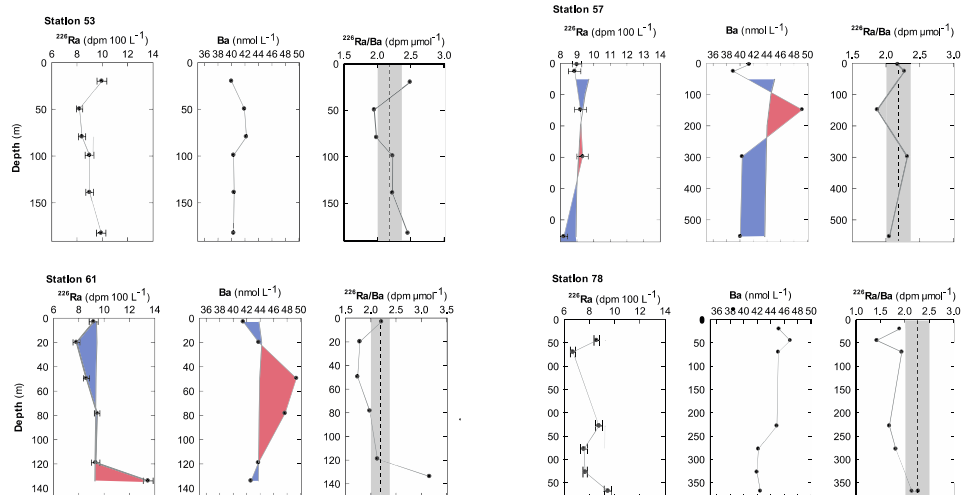




Figure 8

C) Greenland and Newfoundland Margins



D) Labrador Basin

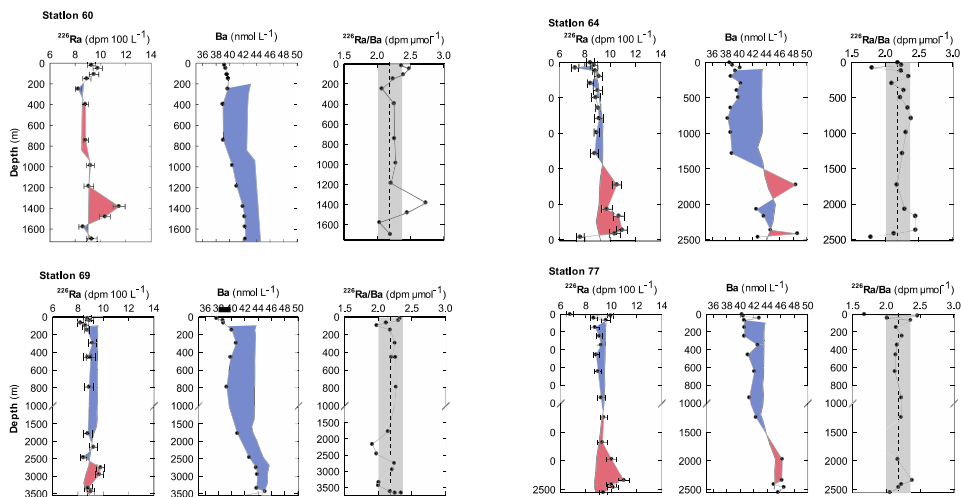




Figure 9

